https://doi.org/10.5194/egusphere-2026-1346
Preprint. Discussion started: 13 April 2026

Drivers of Atmospheric Volatile Methylated Sulfur Variability Across the Southern Ocean and Antarctic Coast

Caleb Mynard[1,2], Emily B. Franklin[2], Joel Alroe[3], Karen Westwood[4,5], Brandon J. McNabb[6], Robert Strzepek[5], Philippe D. Tortell[6], Steven T. Siems[7], Antonio Patti[1], Suzie Molloy[2], Alan Griffiths[8], Branka Miljevic[3], Marc D. Mallet[5], Ruhi Humphries[2], and Erin Dunne[2]

[1]School of Chemistry, Monash University, Melbourne, VIC, Australia
[2]Climate Atmosphere and Ocean Interactions, CSIRO Environment, Melbourne, VIC, Australia
[3]School of Earth and Atmospheric Sciences, Queensland University of Technology, Brisbane, QLD, Australia
[4]Australian Antarctic Division, Department of Climate Change, Energy, the Environment and Water, Hobart, TAS, Australia
[5]Australian Antarctic Program Partnership, Institute for Marine and Antarctic Studies, University of Tasmania, Hobart, TAS, Australia
[6]Department of Earth, Ocean and Atmospheric Sciences, University of British Columbia, Vancouver, BC, Canada
[7]School of Earth, Atmosphere and Environment, Monash University, Melbourne, VIC, Australia
[8]Australian Nuclear Science & Technology Organisation, Lucas Heights, NSW, Australia

Correspondence: Caleb Mynard (caleb.mynard@csiro.au)

Abstract. Biogenic volatile methylated sulfur (VMS) gases, dimethyl sulfide (DMS) and methanethiol (MeSH), are major precursors of climate-cooling sulfate aerosol, yet their sources, co-emission and fate remain poorly constrained over the Southern Ocean and Antarctica. In this study, we combine atmospheric VMS measurements with biogeochemical and meteorological observations from an austral summer Southern Ocean voyage to examine the drivers of atmospheric VMS concentrations across contrasting ocean-atmosphere regimes. At the Antarctic Ice Edge (62–67°S), DMS dominated the VMS burden (up to 5.7 ppb) with episodic coastal polynya and shelf biological hotspots demonstrating very low MeSH:DMS (0.3–4%). In this regime, DMS variability was strongly related to recent air mass exposure to high surface chlorophyll-*a* (R^2 = 0.49), whereas MeSH showed little dependence (R^2<0.14), consistent with stronger heterotrophic control on MeSH production. Over the open ocean (32–62°S), DMS and MeSH were tightly coupled (R^2 = 0.80) with higher MeSH (up to 250 ppt) and MeSH:DMS (∼15%), but chlorophyll-*a* explained little of the variability (R^2 = 0.15); instead, physical ocean structure and boundary-layer conditions influenced VMS variability. DMS and DMSO co-varied at the Antarctic Ice-Edge (R^2 = 0.69), indicating rapid oxidation via addition reactions with hydroxyl and bromine monoxide radicals at the surface. Overall, our results support developing coupled VMS–biogeochemical parameterisations to better capture aerosol–cloud representation in Southern Ocean climate models, and revising DMS-based parameterisations of MeSH at the Antarctic Ice-Edge, which currently appear to overestimate MeSH contributions to the VMS burden under these conditions.

1 Introduction

The ocean-atmosphere exchange of dimethyl sulfide (DMS) represents the largest natural source of biogenic sulfur to the global atmosphere (Simó, 2001; Bates et al., 2004). Produced via enzymatic cleavage of the algal precursor dimethylsulfoniopropi-

https://doi.org/10.5194/egusphere-2026-1346
Preprint. Discussion started: 13 April 2026

onate (DMSP), DMS accounts for up to 70 % of natural sulfur emissions (Lana et al., 2011; Kettle et al., 1999) and exerts strong influence on sulfate aerosol formation, cloud properties, and climate (Charlson et al., 1987; Quinn and Bates, 2011). The Southern Ocean plays a disproportionately important role in this cycle, contributing nearly 60 % of global DMS emissions (Zhou et al., 2024), yet it remains persistently under-observed and poorly represented in models (Mallet et al., 2023a; Hulswar et al., 2022). Co-emitted volatile methylated sulfur (VMS) species, especially methanethiol (MeSH), may also have important climatic impacts, with the Southern Ocean representing an estimated 27 % to global emissions (Wohl et al., 2024; Tashmim et al., 2025). However, the production pathways and atmospheric budgets for MeSH in this region remain poorly constrained, further limiting our understanding of biogenic VMS contributions to Southern Ocean aerosols.

The Southern Ocean provides a rare natural environment where aerosol–cloud interactions are dominated by marine sources, with limited anthropogenic influence (Hamilton et al., 2014; Schmale et al., 2019). Strong spatial and seasonal gradients in sea-ice retreat, iron supply, and mixed-layer depth, lead to highly variable phytoplankton community abundance and structure and therefore biological production of DMSP (McNabb and Tortell, 2023; Sokolov and Rintoul, 2007; Hayward et al., 2024; Heidemann et al., 2024; Wright et al., 2010). These physical–biogeochemical regimes can shift rapidly near the Antarctic coast, giving rise to short-lived but extreme VMS emissions events (Webb et al., 2019; Levasseur et al., 1994; Koga et al., 2014) that remain difficult to capture in coarse climatologies (Ishino et al., 2026).

Chlorophyll-*a* (Chl-*a*) is often used as a proxy for phytoplankton biomass, and therefore as an indirect predictor for DMS (McNabb and Tortell, 2023; Jarníková and Tortell, 2016; Halsey and Giovannoni, 2023; Manville et al., 2023; Zhang et al., 2020). However, ambiguous relationships between DMS and Chl-*a* have been reported in such studies, suggesting additional controls on DMS production, emission, and loss over seasons and regions (Manville et al., 2023). Global surface ocean DMS climatologies (e.g., Kettle et al., 1999; Lana et al., 2011; Jarníková and Tortell, 2016; Hulswar et al., 2022) show their largest discrepancies across the Southern Ocean, where the highest DMS concentrations, particularly those associated with marginal ice zone blooms, are sparsely observed and often omitted. Emerging climatologies for MeSH (Wohl et al., 2024; Tashmim et al., 2025) indicate it may substantially enhance sulfate aerosol burdens, but there are very few seawater and atmosphere MeSH measurements across the Southern Ocean (Lawson et al., 2020; Wohl et al., 2024; Rocco et al., 2025; Mynard et al., 2025b) and MeSH is yet to be routinely incorporated into models, limiting our understanding of its climatic role.

This poses the challenge of understanding whether the more frequently measured seawater and atmospheric DMS can act as a reliable proxy for MeSH emissions, as presented in Wohl et al. (2024); Tashmim et al. (2025); Jacob et al. (2026). Both VMS gases originate from DMSP, but their relative production is highly dependent on phytoplankton taxonomy and physiological state, heterotrophic cycling, and environmental conditions, all of which vary dramatically across the Antarctic ice-edge and the wider Southern Ocean (Hayward et al., 2024). Mynard et al. (2025b) demonstrated a consistently strong relationship between DMS and MeSH over the open Southern Ocean; however, it changes south of the Polar Front along the Antarctic coastline, as a result of unique air-mass histories and contrasting continental, ice-edge, and marine bloom influences that produce distinct MeSH:DMS regimes.

Despite their central role in the sulfur cycle, the fate of VMS species remains incompletely understood. As Figure 1 illustrates, DMS is primarily oxidised by hydroxyl radicals (OH), producing either sulfur dioxide (SO_2) (and ultimately sulfuric

https://doi.org/10.5194/egusphere-2026-1346
Preprint. Discussion started: 13 April 2026

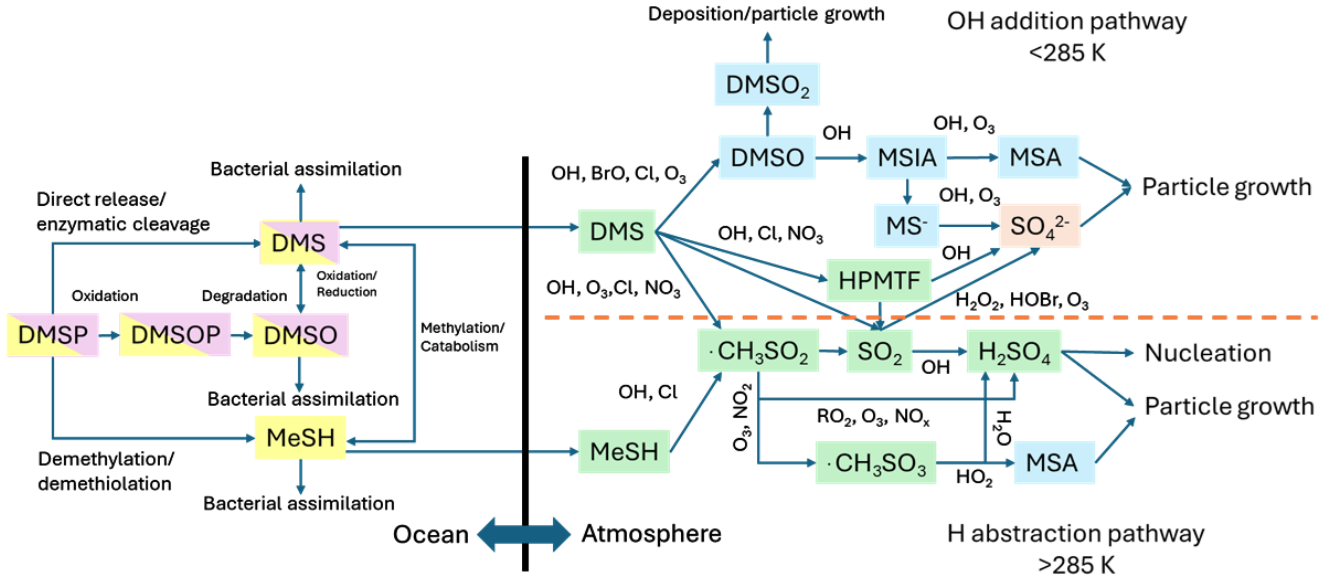

Figure 1. Simplified chemical transformations for climatically relevant pathways of VMS emissons and oxidation. Yellow boxes indicate aqueous phase, pink boxes indicate algal intracellular processing, green boxes indicate gas-phase, blue boxes indicate semi-volatile and red boxes indicate aerosol-phase.

acid) via the H-abstraction pathway, or dimethyl sulfoxide (DMSO) and eventually methanesulfonic acid (MSA) via the OH-addition pathway, with both pathways contributing to sulfate aerosol (Hoffmann et al., 2016; Wang et al., 2021). The branching between these pathways is highly sensitive to temperature and to some extent to halogen chemistry, particularly bromine activation in high-latitude marine boundary layers (Breider et al., 2010; Saiz-Lopez et al., 2007; Read et al., 2008; Jang et al., 2022). MeSH oxidation pathways are incompletely understood, with recent model representation of MeSH emission and oxidation assuming 100 % conversion to SO_2 (Novak et al., 2022; Wohl et al., 2024). However, this may overestimate MeSH contributions to SO_2 at low temperatures. Recent laboratory and modelling studies have provided evidence for non-SO_2 producing MeSH oxidation pathways leading to MSA formation as well as SO_2 and H_2SO_4 (Berndt et al., 2023; Chen et al., 2023; Tashmim et al., 2025); however, the contributions of these pathways to aerosol yields observed in the atmosphere remain uncertain.

Together, these key uncertainties in the polar biogenic sulfur cycle, and the fact that their underlying processes remain underrepresented in current numerical models, underscore the need for high-resolution, co-located measurements of DMS, MeSH, their oxidation intermediates, and the oceanographic drivers that modulate their production. In this study, we present an integrated dataset of atmospheric VMS species, biogeochemical observations, and key environmental observations collected across the Southern Ocean and Antarctic coast during the January–March 2024 austral summer Multidisciplinary Investigations of the Southern Ocean (MISO) voyage. We assess how physical-biological regimes shape VMS variability, evaluate the potential for remotely sensed Chl-*a* to predict atmospheric DMS and MeSH, and explore the degree of coupling between primary VMS

https://doi.org/10.5194/egusphere-2026-1346
Preprint. Discussion started: 13 April 2026

gases and their oxidation products. These observations provide new constraints on VMS source and sink processes and offer insight into how future climatologies and models may better represent biogenic sulfur cycling across the Southern Ocean.

2 Methodology

2.1 Voyage Overview

The MISO (Multidisciplinary Investigations of the Southern Ocean) campaign occurred between 5 January and 5 March 2024 aboard the RV *Investigator*. The voyage departed from Hobart, Australia covering the Southern Ocean from ∼43° S to the Mertz Glacier (67° S), east along the coast of Antarctica (∼150°–113° E) and north along the I9S oceanographic repeat line (115° E) to Fremantle, Australia (31° S). We will focus on the data collected along the Antarctic coastal leg (62–67° S, 113–151° E) here called "Antarctic Ice-Edge" and the northward I9S transect (32–62°, 115° E; Hufford et al. 1997) here called "Open Ocean" (see Figure S4 for the MISO voyage track). From an atmospheric perspective, the MISO voyage aimed to investigate how ocean-ice-biosphere-atmosphere interactions influence aerosols, clouds, precipitation and radiation over the Southern Ocean (Marine National Facility, 2024).

2.2 Measurements of DMS, MeSH and DMSO by PTR-ToF-MS

A Proton Transfer Reaction Time-of-Flight Mass Spectrometer (PTR-ToF-MS 4000, Ionicon Analytik) was deployed to measure volatile organic compounds including DMS, MeSH and DMSO. The DMS and MeSH measurements by PTR-ToF-MS during the MISO voyage have been described previously (Mynard et al., 2025b) and more information is provided in Supplementary Information Text S1. Briefly, ambient air was sampled from the bow mast 18 m above sea level via a heated (40 °C) polyfluoroalkyl (PFA) sample line (42 m, 3/8" I.D.) at a flow rate of ∼7 L min^{-1}. A flow of ∼1 L min^{-1} was drawn off the main inlet via a sample valve switchboard and the PTR-ToF-MS sampled 0.37 L min^{-1} from this flow.

The PTR-ToF-MS was operated with an applied drift tube voltage of 460 V, pressure of 2.6 mbar and temperature of 110 °C (E/N = 132 Td). A mass scan was collected every 10 s and a mass axis calibration was performed every 100 s using a diodobenzene permeation source (PerMaSCal, Ionicon Analytik GmbH, Innsbruck Austria). Measurements of instrument background were attained by directing ambient air via a zero air generator (Parker Balston 75-83, Haverhill, MA) and the calibration and ambient data were background-corrected. Detection limits were 5, 2 and 2 ppt for DMS, MeSH, and DMSO respectively.

The sensitivity of the system to DMS was determined approximately every 5 days during the voyage from measurements with a ∼1 ppm certified gas standard (Apel-Riemer Environmental Inc, CO) diluted with zero air yielding a sensitivity of 518 ± 43 cps ppb^{-1}. MeSH and DMSO were not present in the calibration standard used during the voyage. Instead, MeSH and DMSO sensitivity was derived from post-voyage measurements of certified gas standards containing DMS, MeSH and DMSO (Apel Riemer Environmental Inc, CO). MeSH and DMSO sensitivities of 160 ± 13 cps ppb^{-1} and 88 ± 7 cps ppb^{-1}, respectively, were determined with consistent ratios to DMS of 1:3 (similar to Novak et al. 2022) and 1:6 (similar to Zang and Willis 2025),

https://doi.org/10.5194/egusphere-2026-1346
Preprint. Discussion started: 13 April 2026

respectively. These ratios were then applied to the voyage DMS calibrations to derive scaled sensitivities for MeSH and DMSO. Data were processed and analysed using Ionicon Data Analyzer 2.2.0.7 (IDA, Ionicon Analytik, Innsbruck, Austria, Müller et al. 2013). Air mass contamination by ship exhaust emissions was taken into account by identifying periods of enhanced hydrocarbons ($C_4H_8H^+$, $m/z = 57$) and aromatics (benzene, toluene, and xylene) associated with combustion and such affected data were removed (see more detail in Mynard et al. 2025b). We compared this PTR-ToF-MS-specific exhaust influence to a rolling-window median absolute deviation-based outlier method applied to particle number concentrations (Humphries et al., 2019) and then refined through temporal aggregation and detailed manual inspection of particle size distributions, black carbon, radon, air mass history, and other combustion tracers to produce a final 1-minute exhaust and air mass classification for the entire voyage; the complete methodology of which is presented in Mallet et al., in prep. This filtering method yields minor differences from the concentrations reported in Mynard et al. (2025b), which used a more conservative approach and therefore reported fewer 1-minute DMS and MeSH data (e.g., Mynard et al. 2025b: I9S Transect VMS n $\sim$ 12000 1-min, this study: I9S Transect VMS n $\sim$ 15000 1-min).

2.3 Measurements of Gaseous MSA and Sulfuric Acid by NO_3-CIMS

Gas-phase Methanesulfonic Acid (MSA) and Sulfuric Acid (SA) were measured by a high resolution Chemical Ionisation Mass Spectrometer (Aerodyne Research, MA) employing nitrate reagent ions (NO_3-CIMS). A similar instrument setup has been previously described in Miljevic et al. (2025). Ambient air was sampled from a separate inlet and included a 1.6 m stainless steel 1" line at a flow rate of 60 L min^{-1} followed by a flow of 10 L min^{-1} drawn through 1.2 m of PFA 1/2" tubing to NO_3-CIMS. SA and MSA were quantified from the sum of their respective product ions, normalised to the sum of the reagent ions, and then multiplied by a calibration factor of 8.75×10^9 molecule cm^{-3} ncps^{-1} derived as a median of 21 values reported across studies; which is the same calibration factor determined from Miljevic et al. (2025).

2.4 Measurement of Sulfate Aerosol by ToF-ACSM

Sulfate aerosol (SO_4^{2-}) was measured using a Time-of-Flight Aerosol Chemical Speciation Monitor (ToF-ACSM, Aerodyne Research, MA) fitted with a PM_1 aerodynamic lens and a capture vaporiser. The ToF-ACSM was located in the Aerosol Laboratory in the bow of the ship. Aerosols were sampled from the above bow mast at 180 L min^{-1} to a sample manifold ($\sim$8 m from mast to Aerosol Laboratory sampling manifold, see Humphries et al. 2019), and then via $\sim$3 m, 3/8" copper line at with a flow of 3 L min^{-1} fitted with a Nafion dryer. After which the ToF-ACSM sub-sampled $\sim$84 mL min^{-1}. The instrument was calibrated with 5 mM ammonium nitrate and ammonium sulfate solutions prior to the voyage, yielding an ionization efficiency for nitrate of 84.8 ions pg^{-1}, and relative ionisation efficiency for sulfate of 1.64. A collection efficiency of 1 was applied to the data, which was analysed in Tofware v3.3.0 (TOFWARE AG, Thun, Switzerland) utilising standard fragmentation tables (Allan et al., 2004) to determine mass loading (μg m^{-3}) of sulfate. Minimum detectable limits (MDL) for sulfate of 5 ng m^{-3} were calculated as three times the standard deviation from measurements sampling with a high efficiency particulate air (HEPA) filter connected at the ToF-ACSM inlet.

https://doi.org/10.5194/egusphere-2026-1346
Preprint. Discussion started: 13 April 2026

2.5 Other Atmospheric and Underway Measurements

Ozone (O_3) was measured using two standard Thermo Scientific Model 49i UV photometric O_3 analysers (Thermo Fisher Scientific Inc, Franklin, MA). Both analysers were situated in the Aerosol Laboratory and sampled via 1/4" O.D. PTFE line from the same manifold and inlet described in Sect. 2.4. The meteorological instrumentation has been described previously in Humphries et al. (2019), including measurement of humidity, wind speed and direction (vane and ultrasonic), sea-surface temperature (radiometer), solar radiation (pyranometer), photosynthetically active radiation (PAR), air temperature, air pressure, rain, ozone, and trace gases from port and starboard sensors. The RV *Investigator* has two drop keels that can be lowered 4 m below the hull (about 7-8 m below the waterline) to mount acoustic sensors and transducers; the port keel also contains an inlet for the pumped seawater sampling system. A thermosalinograph (TSG) continuously measures ocean surface temperature, salinity, flow rate, fluorescence, pCO_2, and oxygen (optode). All RV *Investigator* MISO (IN2024_V01) voyage data can be accessed at CSIRO National Collections and Marine Infrastructure (2024).

2.6 Measurements of Biogeochemistry

Seawater DMS, DMSO, and DMSP concentrations were determined via an Organic Sulfur Sequential Chemical Analysis Robot (OSSCAR, Asher et al. 2015) and were quantified using a custom chemiluminescence detector following a similar approach to Nagahata et al. (2013). Full instrument configuration, operating conditions, and calibration procedures are provided in Supplementary Information Text S2. Briefly, DMS was measured and quantified via chemiluminescence after both conversion from DMSP via hydrolysis and from DMSO samples that were electrochemically reduced with a $NiSO_4$ catalyst following a 30-minute protocol (McCulloch and Tortell, 2023). Nitrogen carrier gas delivered the analyte to the reaction chamber, where an ozone–air mixture initiated the chemiluminescence reaction, and the amplified signal was recorded using a dedicated DAQ system.

Total Chl-*a* and phytoplankton community structure as a proportion of Chl-*a* (μg Chl-*a* L^{-1}) were assessed using high-performance liquid chromatography (HPLC) pigment analysis on samples collected from Conductivity, Temperature, Depth instrument (CTD) vertical profile deployments across the entire voyage. Full methodological details are provided in the Supplementary Information S2. Briefly, analyses were conducted following Wright et al. (2010), with chemotaxonomic interpretation performed using the phytoclass R package (Hayward et al., 2023, 2026). Pigment profiles were grouped using hierarchical clustering to account for variability in pigment:Chl-*a* ratios, and phytoplankton classes were then derived via simulated annealing, resolving eight taxa commonly reported for the Southern Ocean namely: diatoms, haptophytes, dinoflagellates, prasinophytes, chlorophytes, cryptophytes, pelagophytes, and cyanobacteria (Fig. S11 and Fig. S12). The ship's underway seawater supply, which had an intake in the ship's drop keel (water depth ~7 m), was equipped with a WETStar fluorometer (Wetlabs, Inc., Philomath, Oregon, USA) that measured Chl-*a* fluorescence at 695 nm (excitation at 460 nm) continuously throughout the voyage. Travel time through the ship's plumbing from intake to the fluorometer was ~1–2 min. We scaled the underway Chl-*a* fluorescence measurements by a correction factor of 3.39, which we derived from total Chl-*a* concentrations measured using HPLC pigment analysis.

https://doi.org/10.5194/egusphere-2026-1346
Preprint. Discussion started: 13 April 2026

2.7 Air Mass Back Trajectory Analysis

To understand the origin of the boundary layer air masses the RV *Investigator* encountered during the voyage, hourly back trajectories were produced using the Lagrangian analysis tool (LAGRANTO version 2.0; Sprenger and Wernli 2015), using hourly 0.25° ERA5 single level and pressure level data. The hourly back trajectories ran for 120 hours and were initialized at 975 hPa. For the purposes of categorising air mass histories encountered during MISO, only the final 12 h prior to arrival were retained, representing the most recent atmospheric transport history influencing surface observations on the time scales of VMS emission and oxidation processes. Air masses were categorised according to latitude and exposure to biological productivity. The ERA5 land-sea mask was used as a proxy for surface type (<0.1 is oceanic, >0.1 is land/ice). Trajectories were classified into three broad spatial categories: Antarctic, Australian, and oceanic. Trajectories with an average latitude south of 62°S and over regions with high land/ice fraction (>0.1) were defined as Antarctic, indicating continental/sea ice influence (Humphries et al., 2021; Mallet et al., 2025; Mynard et al., 2025b). Trajectories with an average latitude north of 45°S with high land fraction (>0.1) were defined as Australian, indicating anthropogenic influence. All remaining trajectories were classified as oceanic and spanned 34–67°S.

Back trajectories were combined with monthly satellite products of chlorophyll-*a* (Chl-*a*, in μg m^{-3}) and sea surface temperature (SST, in °C) at 0.1°× 0.1° spatial resolution from the Moderate Resolution Imaging Spectroradiometer (MODIS) Aqua sensor (NASA Earth Observations, 2025). This was repeated using daily ocean mixed layer depth (MLD, in m) fields at 0.125°× 0.125° resolution from the ARMOR3D NRT–TSHUVMld Global Ocean Observation-based product (Buongiorno Nardelli, 2020). The cumulative boundary layer Chl-*a* exposure was then calculated for each back trajectory by summing the Chl-*a* value along each point when the trajectory was most recently below the ERA5 atmospheric boundary layer height. A sensitivity test of multiple backward trajectory durations (12-120 hours) confirmed that restricting air mass back trajectories to 12 hours demonstrated the strongest relationship with VMS species, while distinguishing air mass spatial category consistent with the time scales of VMS emission and oxidation processes (Arnold et al. 2010; Novak et al. 2022; see Fig. S3). This cumulative Chl-*a* was used as a proxy for biological productivity, divided into high or low productivity based on the median cumulative Chl-*a* (1.23 μg m^{-3}). This approach generated six trajectory categories based on 12-hour cumulative boundary layer Chl-*a* used for later analyses: Antarctic high productivity, Antarctic low productivity, Australian high productivity, Australian low productivity, Oceanic high productivity, and Oceanic low productivity. For the purposes of the current study, only Oceanic and Antarctic air mass influences were considered within the scope of the following analysis.

3 Results and Discussion

3.1 Overview of Atmospheric VMS Observations Across the Southern Ocean

Air masses sampled along the Antarctic Ice-Edge (62–67°S) and the Open Ocean (32–62°S) legs traversed during the MISO voyage exhibited unique characteristics in their exposure to marine biologically productive regions, and their associated primary VMS concentrations and oxidation product regimes (Fig. 2). The transit down to the Antarctic coast (5–10 Jan; Fig. 2)

https://doi.org/10.5194/egusphere-2026-1346
Preprint. Discussion started: 13 April 2026

was excluded from analyses here as data were significantly impacted by ship exhaust contamination, compared to the extensively measured I9S Transect. The latitudinal gradients of atmospheric DMS and MeSH from this voyage have been previously described in Mynard et al. (2025b).

Briefly, very high biological productivity in summer along the Antarctic Ice-Edge transect (marine in-situ underway Chl-*a* up to 5 μg L^{-1}, >62°S) coincided with the highest atmospheric concentrations of DMS, with extreme spikes up to 5.7 ppb and median concentrations of 340 ppt (Fig. 3). In comparison, MeSH concentrations were up to 200 ppt (median = 23 ppt, Fig. 2) over the same spatial regions. Lower biological productivity was observed along the latitudinal transects over the Open Ocean (marine *in-situ* underway measured Chl-*a* <1 μg L^{-1}), where DMS and MeSH were more tightly coupled (R^2 = 0.80, slope = 0.173, $p < 0.05$) ranging from below detection limits (BDL) to 1.4 ppb (median = 271 ppt) and BDL to 253 ppt (median = 28 ppt), respectively.

In line with the VMS oxidation schematic illustrated in Fig. 1, higher concentrations of gas-phase DMSO were observed across the Antarctic Ice-Edge (up to 84 ppt, Fig. 2 and Fig. 3) and showed strong coherence with DMS. Elevated gaseous MSA concentrations (up to 1.5×10^8 molecules cm^{-3}; Fig. 2) did not coincide with precursor VMS levels and suggest evaporation from MSA-containing aerosols and long-range transport from the Antarctic continent (Miljevic et al., 2025; Mallet et al., 2025). Sulfuric acid concentrations were highest at warmer low latitudes (up to 1.3×10^6 molecules cm^{-3}, <45° S).

3.2 Influence of Air Mass History on Atmospheric VMS Composition

To investigate VMS variability within the two broad spatial regions of the Southern Ocean and Antarctic coast, we classified the sampled air masses into four categories (oceanic low productivity, oceanic high productivity, Antarctic low productivity and Antarctic high productivity). Air mass history classification was based on 12-hour back trajectory air mass origin and boundary layer cumulative Chl-*a* (hereafter cBLChl-*a*), with the median of Chl-*a* = 1.23 μg m^{-3} used as the threshold to define air mass contact with low and high biological productivity surface ocean regions (Sect. 2.7).

Along the Antarctic Ice-Edge transect, air masses sampled based on only the recent 12 hours of back trajectories were predominantly of oceanic origin (83 %; Fig. S5) and across both oceanic and Antarctic continental origins, they were mostly characterised as high productivity (78 %; Fig. S5). Air masses originating from the Antarctic continent traversed coastal biologically productive waters for shorter periods (<2 hours over a productivity regime within each trajectory) relative to air masses with prolonged exposure to active phytoplankton blooms along the Antarctic shelf region classified within the oceanic high productivity regime (>5 hours over the productivity regime within each trajectory). Along the I9S Transect (Open Ocean) transect, air mass origins were purely oceanic and predominantly low productivity (81 %, Fig. S5). Air masses generally originated from westerly winds over the Southern Indian Ocean region, with the highest productivity air masses sampled over the Subtropical Front (42–52°S; Fig. S4).

Air masses originating over regions of high biological productivity had consistently higher VMS concentrations. In oceanic high productivity and Antarctic high productivity air masses, median concentrations were found to be 384 and 786 ppt of DMS, respectively, 36 and 45 ppt of MeSH, respectively, and 29 and 79 ppt of DMSO, respectively (Fig. 3). In oceanic low

https://doi.org/10.5194/egusphere-2026-1346
Preprint. Discussion started: 13 April 2026

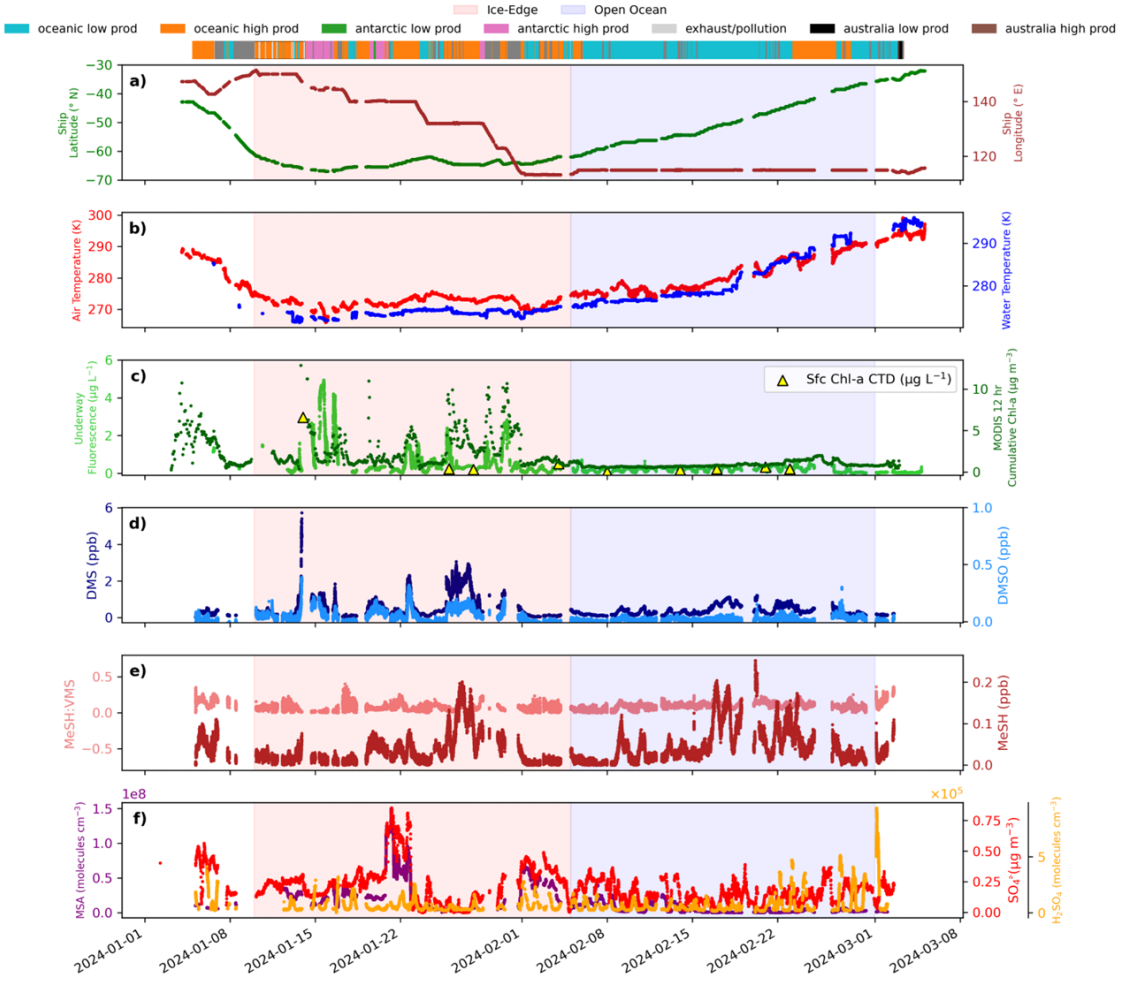

Figure 2. MISO voyage time series of *in-situ* measurements and derived product variables from satellite/model outputs. (a) *RV* Investigator ship latitude/longitude (green/brown), (b) *RV* Investigator measured air (red) and sea surface (blue) temperature, (c) MODIS 12-hour cumulative Chl-*a* (dark green), scaled underway *in-situ* fluorescence as a proxy for Chl-*a* (light green) and surface layer Chl-*a* measured from Conductivity, Temperature, and Depth instrument measurements (yellow triangles, left axis), (d) gas-phase volume mixing ratio DMS (navy) and DMSO (light blue), (e) gas-phase volume mixing ratio MeSH (dark red) and MeSH:DMS (light red), (f) gas-phase number density MSA (purple), sulfuric acid (orange) and aerosol-phase mass loading sulfate (red). The highlighted red section indicates the Antarctic Ice-Edge region and the blue section indicates the Open Ocean (I9S Transect) region. The colour bar at the top of the figure represents the air mass category based on coupled cumulative Chl-*a* (a proxy for low/high biological productivity) and 12 hour air mass backward trajectories. The colour bar also indicates data removed due to contamination from ship exhaust and transported pollution where the PTR-ToF-MS was usually changed to calibration and zero measurements (grey). Other breaks in the time series data indicate instruments were offline from ambient measurement or data were removed during quality control procedures.

https://doi.org/10.5194/egusphere-2026-1346
Preprint. Discussion started: 13 April 2026

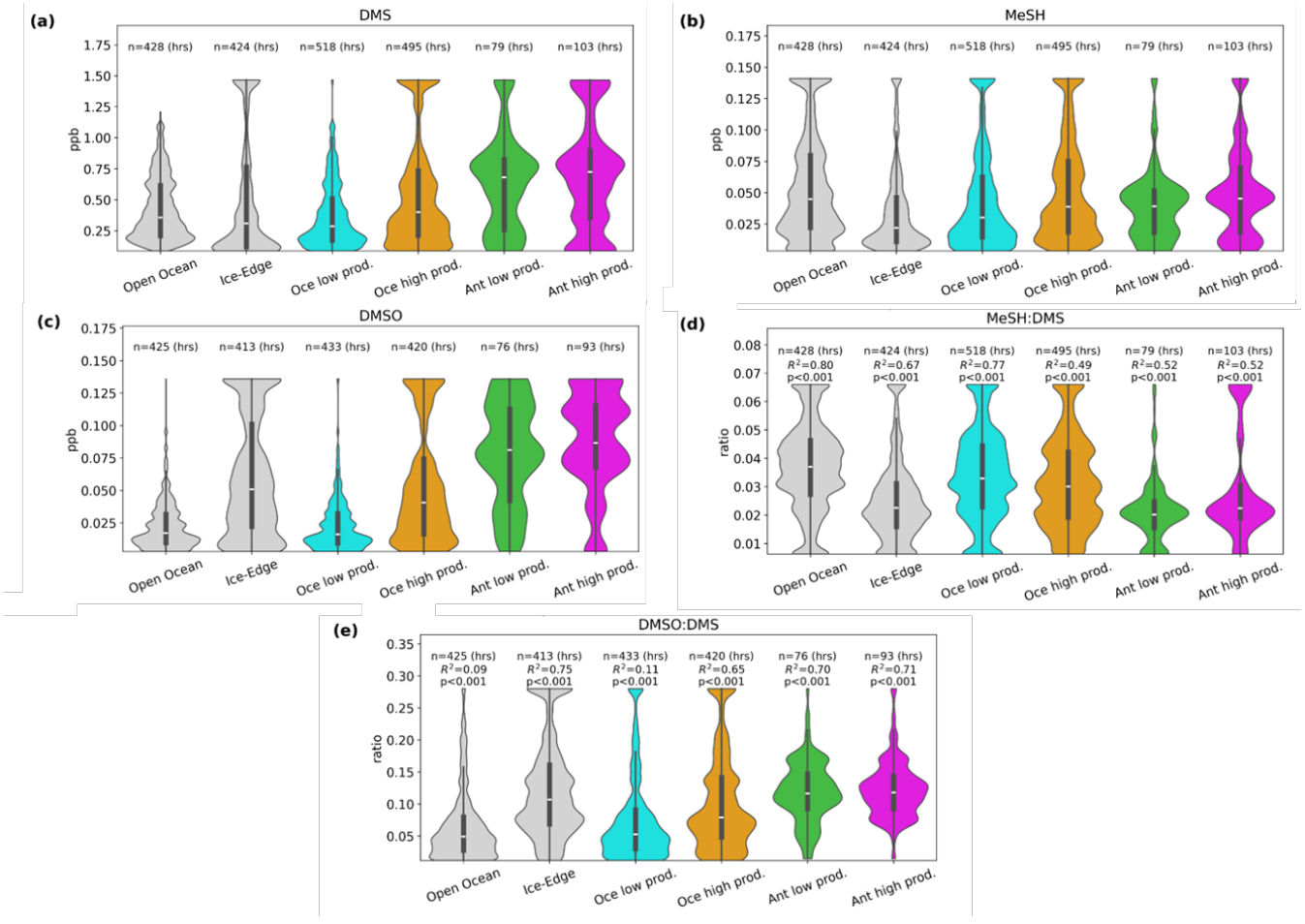

Figure 3. Violin plots of 5th-95th percentile data for (a) DMS, (b) MeSH, (c) DMSO, (d) MeSH:DMS and (e) DMSO:DMS. The median value is given by the white line within each boxplot and the whiskers span 1.5×IQR. Data are categorised by ship location (grey), oceanic low productivity (blue), oceanic high productivity (orange), Antarctic low productivity (green) and Antarctic high productivity (pink). N is the number of trajectory points in hours from each 12 hour air mass backward trajectory ran for each hour along the voyage. Coefficient of determination between MeSH and DMS (d), and DMSO and DMS for each air mass category (e).

https://doi.org/10.5194/egusphere-2026-1346
Preprint. Discussion started: 13 April 2026

productivity and Antarctic low productivity air masses, median concentrations were generally lower with 232 and 657 ppt for DMS, respectively, 24 and 33 ppt for MeSH, respectively, 14 ppt and 77 ppt for DMSO, respectively (Fig. 3).

3.3 Predictors of VMS Variability at the Antarctic Ice-Edge versus the Open Ocean

Next, we explore whether air mass history, in-situ observations, and trajectory-integrated metrics can explain and predict variability in VMS composition within Antarctic and oceanic air masses. A consistent co-varying relationship between DMS and cBLChl-*a* occurred over the Antarctic Ice-Edge, which was especially driven by the oceanic high productivity air masses (R^2 = 0.49, n = 92, slope = 0.21, $p < 0.01$), as illustrated in Figure 4. In fact, 6-hourly back trajectories demonstrated the strongest DMS–cBLChl-*a* relationship in this region (Fig. S3); however, we use 12-hourly because it offers improved differentiation between Antarctic coastal and continental influence (Sect. 2.7). This DMS–cBLChl-*a* coupling was significantly stronger than for DMS and measured *in-situ* Chl-*a* ($R^2 < 0.05$). Likewise, for 12-hour back trajectory averaged Chl-*a* ($R^2 < 0.1$) and >12-hour back trajectory cumulative Chl-*a* ($R^2 < 0.2$) over both transects. Given the abundance of high DMSP- and DMS-producing phytoplankton species and shallow MLDs encountered along the Antarctic coastal transect (Simó and Dachs, 2002), it is unsurprising we observed a close coupling between atmospheric DMS and cBLChl-*a* in the high productivity Antarctic air masses (Sect. 3.3). Perhaps more notably, for the Antarctic coastal regions, cBLChl-*a*, derived from monthly MODIS retrievals and 12-hour back trajectories, was able to reproduce the time-varying behaviour of atmospheric DMS occurring on the order of hours (Fig. 4). Consistent with rapid DMS oxidation via OH-addition or bromine monoxide radical (BrO) oxidation at the Antarctic Ice-Edge (Fig. 1), DMSO strongly co-varied with DMS under this temperature regime (R^2 = 0.7, slope = 0.07, $p < 0.01$, Figure 3e) and therefore was also tied to cBLChl-*a* (R^2 = 0.29, n = 443, $p < 0.01$).

Despite the moderately strong correlation between atmospheric MeSH and DMS at the Ice-Edge (R^2 = 0.67, $p < 0.001$, using 5th–95th percentile data; Fig. 3d), MeSH did not show as close a relationship with cBLChl-*a* ($R^2 < 0.14$; Fig. S16). Moreover, MeSH:DMS correlation was the same in both Antarctic high- and low productivity air masses, indicating that Chl-*a* was not a common predictor of the coupling between MeSH and DMS at the Antarctic Ice-Edge (Fig. 3d). This is likely attributable to the dominance of heterotrophic processes involved in DMSP conversion to MeSH and not primary production, as is the case for DMS (Sect. 3.5, Fig. S9, Fig. S10 and Fig. S12). These findings indicate that, in the context of summertime ice-edge conditions, even low time resolution remote sensing ocean optical properties, used to construct our cBLChl-*a* metric, may be a sufficiently robust predictor of atmospheric DMS emissions, but not for atmospheric MeSH emissions. This has the potential to significantly improve prediction of extreme atmospheric DMS dynamics, which remain a key challenge for polar sulfur chemistry models (Ishino et al., 2026).

Over high productivity regimes, other *in-situ* measurements and back trajectory variables including wind speed, air and sea surface temperature, humidity, ozone and boundary layer height, explained less than 20 % of the variance in DMS (Fig. S6). However, removing the biological source influence by analysing residuals after accounting for the cBLChl-*a* resulted in in-situ wind speed explaining up to 36 % of the residual variance in DMS and up to 52 % of the residual variance in MeSH. Although a negative association between Chl-*a* concentration and MLD was generally observed (Fig. S7), no direct linear relationship

https://doi.org/10.5194/egusphere-2026-1346
Preprint. Discussion started: 13 April 2026

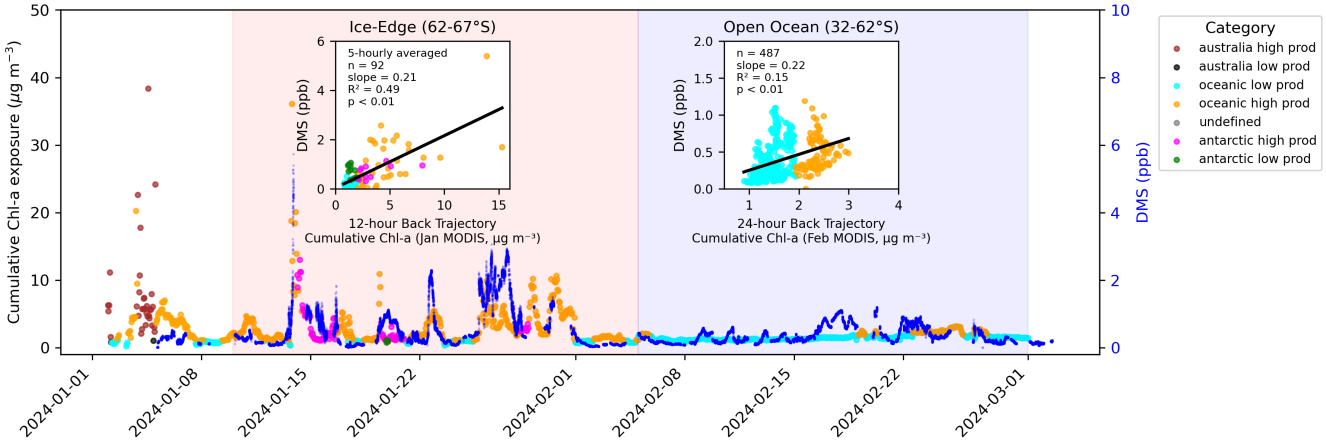

Figure 4. Time series of atmospheric DMS concentrations (blue data points), 12-hour back trajectory cumulative boundary layer Chl-*a* (Jan 2024 MODIS) over Antarctic Ice-Edge (red highlighted region) air mass history categories (coloured data points), and 24-hour back trajectory cumulative boundary layer Chl-*a* (Feb 2024 MODIS) over Open Ocean (blue highted region) air mass history categories. Regression scatter plots of DMS versus cumulative Chl-*a* exposure are included over the Ice-Edge (left) and Open Ocean (right) periods. The Ice-Edge data points area averaged to 5-hourly resolution to optimise the regression, as the outliers significantly change the correlation in the 1-hourly data (see further in Sect. 3.5.)

was identified between these variables within the high productivity regimes at the Antarctic Ice-Edge ($R^2 < 0.07$; Fig. S7). Neither was there a correlation between MLD (or Chl-*a*:MLD) and DMS ($R^2 < 0.05$; Fig. S6; Fig. S7).

In contrast to the Antarctic Ice-Edge where cBLChl-*a* was a reliable predictor of atmospheric DMS variability, cBLChl-*a* was a poor indicator over Open Ocean regimes (Fig. 4), where the DMS–cBLChl-*a* relationship was weaker ($R^2 = 0.15$, n = 487, slope = 0.22, $p < 0.01$) and an optimal relationship occurred using 24-hourly back trajectories (Fig. 4 and Fig. S3). North of the oceanic Polar Front, the absence of land barriers and the influence of the Antarctic Circumpolar Current create a more heterogeneous ocean surface with weaker, more dispersed, and often deeply mixed biological sources (Sokolov and Rintoul, 2007; Goosse et al., 2025). The dominant taxa are often weaker DMSP producers compared to polar bloom species (Teng et al., 2021; Asher et al., 2017), especially when compared to those observed at the Ice-Edge (Sect. 3.5). Relative to the shallower bathymetry and shallower MLDs in Antarctic shelf regions, where total Chl-*a* consistently peaked and thus cBLChl-*a* best predicted DMS (Fig. 4; Sect. 3.5, Fig. S6 and Fig. S9), MLDs over the Open Ocean were consistently deeper and phytoplankton biomass occurred at greater depths (Sect. 3.5; Fig. S12; i.e., 80 m along the I9S transect versus 5 m at the MPA). The MODIS Aqua satellite retrieves only near-surface concentrations of Chl-*a* (NASA Earth Observations, 2025), and therefore may not accurately represent total phytoplankton biomass in the bulk water over the Open Ocean region (34–62° S).

The Open Ocean region was characterised by generally weak and inconsistent coupling between atmospheric VMS concentrations and the range of meteorological, oceanographic, and biological variables examined (Fig. S6). However, consistent with previous studies reporting the effect of open ocean slope transitions on biological sources (Shadwick et al., 2017; Hayward

https://doi.org/10.5194/egusphere-2026-1346
Preprint. Discussion started: 13 April 2026

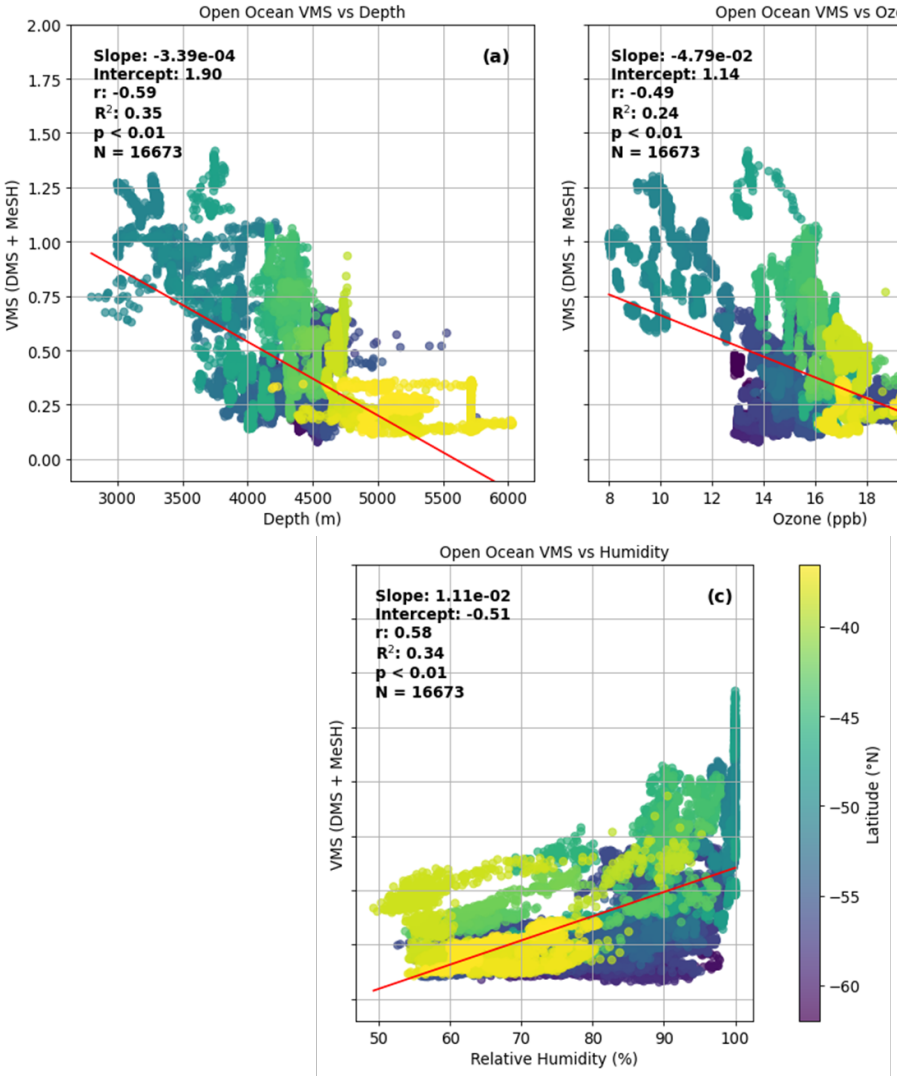

Figure 5. Atmospheric VMS relationships with ocean/seafloor depth (a), *in-situ* ozone (b), and *in-situ* relative humidity (c) over the Open Ocean region (34–62° S).

https://doi.org/10.5194/egusphere-2026-1346
Preprint. Discussion started: 13 April 2026

et al., 2024), Figure 5a illustrates that measured seafloor depth explained 35 % of the variance of our atmospheric VMS observations. The highest observed VMS concentrations occurred at the shallowest ocean depths, especially MeSH at the Subtropical Front (>200 ppt, <4000 m; Fig. 5a). MLD exhibited a substantially stronger correlation with Chl-*a* along the Open Ocean transect than at the Antarctic Ice-Edge (R^2 = 0.35; Fig. S7); however, no direct correlations were observed between MLD and DMS over the Open Ocean (R^2 < 0.01, p = 0.7; Fig. S7) or the Antarctic Ice-Edge (R^2 = 0.06, p < 0.01; Fig. S7). While we found that cBLChl-*a* and MLD were moderately correlated over the Open Ocean (R^2 = 0.37), we did not observe a consistent relationship between these variables and atmospheric VMS (R^2 < 0.1; Fig. S6) unlike other previous research that has shown a correlation between seawater DMS and MLD as well as DMS and Chl-*a*:MLD relationships (Simó and Dachs, 2002; Simó and Pedrós-Alió, 1999; McNabb and Tortell, 2023; Jarníková and Tortell, 2016). Despite this, we observed a moderately strong inverse relationship between VMS concentrations and measured bathymetry (R^2 = 0.35, Fig. 5), a pattern not observed over the region we define here as the Antarctic Ice-Edge. However, this relationship likely reflects the indirect influence of large-scale circulation and associated air mass history rather than a mechanistic control on VMS production or emission. Atmospheric factors that co-varied with VMS over the Open Ocean included ozone (Fig. 5b), relative humidity (Fig. 5c), back trajectory specific humidity and air temperature (Fig. S6), which together explained ∼25–50 % of the variance in VMS.

The absence of a robust predictor suggests that Open Ocean region atmospheric VMS variability emerges from the integration of heterogeneous source regions, transport, and atmospheric processing, rather than being governed by clearly identifiable source-related drivers like those observed at the highly biologically-mediated Antarctic Ice-Edge. Unlike the shallow, highly stratified polar waters, the deep offshore water column of the Open Ocean is shaped by large-scale oceanographic processes rather than local biological production, indicating it was not as strongly source-driven by local surface-ocean processes as what was observed at the Antarctic Ice-Edge. Along the I9S transect (115° E) measured during this voyage, previous work by McCartney and Donohue (2007) demonstrated that the water column is influenced by deep potential-vorticity maxima and enhanced mixing where dense western-boundary waters interact with lighter Antarctic Circumpolar Current waters.

3.4 Spatial Variability in Atmospheric MeSH:DMS Ratios

Spatial patterns in the atmospheric MeSH:DMS ratio provide insight into how underlying DMSP cycling and atmospheric processing modulate VMS speciation across the Southern Ocean regimes. As first presented in Mynard et al. (2025b), atmospheric MeSH:DMS ratios showed pronounced spatial variability, with lower and more variable ratios observed along the Ice-Edge (∼0.05) than over the Open Ocean (∼0.15), and lower than previously reported from other Southern Ocean data sets collected at lower latitudes (∼0.13–0.19; Lawson et al. 2020; Rocco et al. 2025). The low atmospheric MeSH:DMS ratios that we measured at the Antarctic Ice-Edge are more consistent with ratios of ∼0.02 reported from measurements of dissolved MeSH and DMS in coastal waters west of the Antarctic Peninsula (Berresheim, 1987), and median atmospheric ratios <0.1 reported from Northern Hemisphere high latitudes (Ishino et al., 2026). These lower and more variable MeSH:DMS ratios may have implications for modelling studies which have used global seawater DMS climatologies and the relationship between MeSH and DMS to construct estimates of oceanic MeSH (Tashmim et al., 2025; Wohl et al., 2024; Jacob et al., 2026). These modelling

https://doi.org/10.5194/egusphere-2026-1346
Preprint. Discussion started: 13 April 2026

studies have used MeSH:DMS ratio scaling factors on the order of 0.1–0.2, which likely resulted in an overestimation of MeSH emissions for regions such as the Antarctic Ice-Edge.

In contrast to the air masses encountered at the Antarctic Ice-Edge, the Open Ocean air masses exhibited a consistent coupling between DMS and MeSH (Fig. 3d; Mynard et al. 2025b), yet their distributions are largely decoupled from surface chlorophyll biomass (Fig. 4 and Fig. S6). This is because DMS and MeSH largely share a common biogenic origin from marine DMSP cycling and experience relatively homogeneous atmospheric processing. At the Antarctic Ice-Edge, the MeSH:DMS relationship is more complex, as discussed in the next Sect. 3.5.

The atmospheric MeSH:DMS ratios observed over the Open Ocean (∼0.15) in this study are consistent with the 0.13–0.19 ratios reported from other Southern Ocean data sets collected at lower latitudes (Lawson et al., 2020; Rocco et al., 2025; Mynard et al., 2025b) and the ∼0.1–0.2 ratios reported from other ocean regions (Novak et al., 2022; Tashmim et al., 2025; Wohl et al., 2025; Kilgour et al., 2025). Consistent with this coupling under low-productivity conditions (where cBLChl-*a* does not dominate variability in this study), nocturnal accumulation periods over the Open Ocean yielded sea–air flux estimates of 15–124 ng m^{-2} s^{-1} for DMS and 0.1–17 ng m^{-2} s^{-1} for MeSH (Supplementary Information Text S4; Tables S1 and S3), with a broadly variable MeSH:DMS flux ratio (0.008–0.462) that generally exceeded recent southwest Pacific nocturnal accumulation estimates (Lawson et al., 2020; Rocco et al., 2025). However, the increase in atmospheric MeSH:DMS with increased SSTs observed in this study, especially over the Subtropical Front (Fig. S15), is not consistent with the trend determined in a previous global synthesis of seawater MeSH and DMS concentrations (Wohl et al., 2024), which reported lower MeSH:DMS ratios (∼0.1) associated with SSTs above a threshold of 8–12° C, and higher MeSH:DMS (∼0.3) at lower SSTs; nevertheless, that analysis was based on very limited data from these latitudes of the Southern Ocean.

3.5 Case Studies of Enhanced VMS: Biological Drivers and Speciation

Having identified the spatial patterns in atmospheric DMS and MeSH concentrations and the key predictors of their variability across the Antarctic Ice-Edge and Open Ocean regions, we now investigate selected case studies to gain process-level insights into how Southern Ocean and Antarctic coastal oceanographic and biological features influence atmospheric DMS and MeSH production and emission. Extreme seawater DMS concentrations, in excess of 100 nM, have been reported in Antarctic coastal waters associated with springtime sea ice break up that releases trapped DMS/P and seeds subsequent intense phytoplankton blooms that can persist throughout the summer (Webb et al., 2019; Stefels et al., 2018; Trevena and Jones, 2006). The spatial and temporal heterogeneity in VMS emissions introduced by these hotspots is not well represented in models, which instead often implement open ocean derived fluxes (Ishino et al., 2026). Furthermore, current models do not account for MeSH, which growing evidence suggests also plays an important role in aerosol formation and the oxidative capacity of the atmosphere (Novak et al., 2022; Wohl et al., 2024). Modelling efforts to date have exploited the typically close coupling between DMS and MeSH to derive global MeSH emission fields from DMS climatologies (Wohl et al., 2024; Tashmim et al., 2025; Jacob et al., 2026). However, as mentioned above, although the MeSH:DMS ratios over the Southern Ocean are relatively consistent (10–35 %), they vary seasonally and are much lower (<5 %) and more variable at the Antarctic coast (Mynard et al., 2025b).

https://doi.org/10.5194/egusphere-2026-1346
Preprint. Discussion started: 13 April 2026

We observed two distinct episodes at the Antarctic coast with extreme atmospheric VMS concentrations, up to 25 times the MISO voyage medians, which were associated with oceanic and Antarctic high productivity air masses sampled over intense blooms at the Mertz Polynya (MPA), and at a process station (PS2) along the continental slope. In both case studies, atmospheric concentration dynamics were predominantly source driven, rather than significantly controlled by atmospheric loss processes. This is supported by the close coupling between air mass DMS concentrations and exposure to phytoplankton biomass as indicated by monthly MODIS Chl-*a* (Fig. 4) along with the high dissolved concentrations of DMS at the MPA (Fig. S11; dissolved DMS measurements were not available at PS2). Wind speeds and water temperatures in both case studies were not outside of normal ice-edge conditions (Fig. 2 and Fig. S13), suggesting that high atmospheric VMS concentrations and concentration ratios are therefore considered indicative of water-side processes. A third period of atmospheric VMS enhancements occurred at the biologically productive Subtropical Front region.

3.5.1 The Mertz Polynya Area (65.33–67° S, 140–150° E)

The first extreme event occurred over 12–17 Jan 2024, with atmospheric DMS concentrations up to 5.7 ppb (>q95), with associated MeSH concentrations of 90 ppt and exhibited moderately strong MeSH:DMS relationships (R^2 = 0.58) yet a very low MeSH:DMS of 0.4 %. These air masses were of mixed oceanic and Antarctic high productivity origins that had recently passed over the intense phytoplankton blooms in the Mertz Polynya Area (MPA; 65.33–67° S, 140–150° E). The MPA is a shallow, stratified, post-calving polynya system where enhanced light exposure and sea-ice circulation support intense phytoplankton blooms even in late summer (Shadwick et al., 2017). This East Antarctic polynya system has been the subject of recent dramatic changes in dynamics and biogeochemistry following the 2010 calving of the Mertz Glacier Tongue (Shadwick et al., 2013). In November 2023, sea-ice extended to ∼63° S covering most of the MPA before retreating through December and the subsequent melt exposed the MPA in January 2024 shortly before the MISO voyage (MODIS Aqua, Fig. S8). During MISO, the RV *Investigator* transited over a shallow (<500 m) Antarctic continental shelf region of the MPA characterised by decreased surface salinity (33.8 PSU) and sub-zero water temperatures (< -1° C) (Fig. S9). Depth profiles of temperature and salinity from CTD sampling showed a very shallow surface MLD of ∼10 m (Fig. S12). Based on MODIS Chl-*a* the MPA bloom intensified during January and dissipated by late February (Fig. S8). The ship was stationary for 3 days close to a summer retreating sea ice region of very high biological productivity. Chl-*a* from *in-situ* surface fluorescence measurements was up to 5 μg L^{-1} (Fig. 2). Laboratory pigment analysis from CTD vertical profile sampling showed a ∼3 μg L^{-1} Chl-*a* band extending from the surface to ∼30 m depth (Fig. S12a). Within the surface to 30 m, phytoplankton community composition as a fraction of Chl-*a* showed a high abundance of haptophytes (3×median) and dinoflagellates (5×median), known strong DMS/P producers (Fig. S11 and S12). Diatoms were the dominant phytoplankton class (32×median), which in high abundance can also be important dissolved DMS/P producers in sea ice regions (Sheehan and Petrou, 2019). This period also coincided with high dissolved DMS/P concentrations (>100 nM, Fig. S11) and elevated seawater DMSO (>10 nM) which correlated strongly with seawater DMS (R^2 = 0.78, $p < 0.01$, n = 35). Chromophoric dissolved organic matter (CDOM) was low at the surface (<1.5 ppb), but increased to >2 ppb below ∼100m depth (Fig. S12). Low levels of CDOM may imply less DMS loss via both CDOM-mediated photolysis (Taalba et al., 2013) and lower bacterial DMS consumption (Piontek et al., 2021).

https://doi.org/10.5194/egusphere-2026-1346
Preprint. Discussion started: 13 April 2026

The shallow mixed layer, very high biological productivity, and elevated light conditions experienced at the MPA likely favoured direct DMS production by phytoplankton, especially haptophytes such as *Phaeocystics* sp., and explains the close coupling between DMS and air mass cumulative Chl-*a* exposure in this region (Stefels and van Boekel, 1993; Simó and Pedrós-Alió, 1999; Teng et al., 2021; Sun et al., 2016; van den Berg et al., 1996). DMSO reduction may have been an additional important pathway of DMS production at the MPA. Seawater dissolved DMSO is produced primarily through the photochemical and biological oxidation of DMS (Spiese et al., 2009; Brimblecombe and Shooter, 1986; Hopkins et al., 2023) and, to a lesser extent, via direct release from DMSP-containing phytoplankton, such as dinoflagellates, diatoms and haptophytes (Simó et al., 2000, 1998). High concentrations of dissolved DMSO observed at the MPA have also been observed elsewhere in Antarctic waters (Trevena and Jones, 2006; Tison et al., 2010), associated with the haptophyte *Phaeocystis antarctica*. Although primarily recognised for its high DMSP production, *P. Antarctica* has also been reported to contain and release DMSO (Asher et al., 2011, 2017). While substantial DMSO production is more commonly attributed to oxidative and microbial processes (Spiese et al., 2009), Asher et al. (2011) showed that intense microbial activity in Antarctic sea-ice environments promotes significant DMS production via rapid DMSO reduction and DMSP cleavage, suggesting that this rapid biological DMSO reduction can dominate DMS production across diverse Antarctic sea-ice environments.

The overall biological pathways driving phytoplankton production of DMS/P/O are considered to be at least partly driven by physiological stress where phytoplankton may produce DMS/P/O as a cryoprotectant, osmoregulator, or in response to oxidative stress (Vance et al., 2013; McNabb and Tortell, 2025; Kirst et al., 1991). It is plausible the production of these sulfur species was upregulated in the prevailing conditions at the MPA where the spring/summer sea-ice retreat results in rapid changes in temperature, UV, salinity and nutrient availability. Polar diatoms in very high abundance, as was the case for the MPA (Fig. S12c), are typical of summertime blooms in this region and can also significantly contribute to the pool of DMS/P (Sheehan and Petrou, 2019). It is also possible sea-ice algae and their DMS/P/O metabolites further added to the DMS pool at the MPA during the January sea-ice retreat (Tison et al., 2010). However, the open water conditions during sampling and the close coupling between MODIS Chl-*a* and DMS observed suggest that while sea-ice algae may have seeded the blooms encountered during MISO, *in-situ* production via the aforementioned pathways were the dominant source of enhanced DMS observed at the MPA. The very low MeSH:DMS ratio of 0.4 % at the MPA compared to ∼15 % over the Open Ocean is largely due to the very intense DMS emissions, but may also be a consequence of the shallow MLD resulting in UVB-photoinhibition of heterotrophic bacterioplankton and lower bacterial sulfur demand limiting MeSH production (Simó and Pedrós-Alió, 1999).

3.5.2 Process Station 2 (64° S, 132° E)

A second episode during the period 26–28 Jan 2024, referred to here as Process Station 2 (PS2), was characterised by high atmospheric mixing ratios of both DMS (up to 3.1 ppb, >q90) and MeSH (up to 200 ppt, >q95) (MeSH:DMS = 3 %). PS2 occurred when the ship was stationary to the north-west of the MPA (64° S, 132° E) in a deeper (>1500 m), warmer (>0° C) open-ocean region over the continental slope (see Fig. S8). Depth profiles of temperature and salinity from CTD sampling showed a moderately shallow mixed layer ∼17 m (Fig. S12). The sampled air masses were predominantly easterly, traversing biologically productive pelagic and Antarctic coastal regions for extensive periods during 26–27th Jan. This period

https://doi.org/10.5194/egusphere-2026-1346
Preprint. Discussion started: 13 April 2026

was characterised by cloudy conditions (low photosynthetically active radiation) and rainfall (Fig. S13), which may have limited photo-inhibition of bacterioplankton resulting in slightly higher atmospheric MeSH concentrations associated with air masses from this region compared to the MPA. Note that the rapid increase in atmospheric DMS (∼3 ppb) and MeSH (∼100 ppt) around 22–23 Jan 2024 (Fig. 2) occurred when air masses were directly downwind of the biologically productive PS2 region. The PS2 region had lower surface Chl-*a* compared to the MPA from *in-situ* surface fluorescence measurements (up to 2 μg L^{-1}). CTD depth profiles showed an increase in Chl-*a* from 0.2 μg L^{-1} at the surface (5 m) to a peak of 0.65 μg L^{-1} at ∼55 m depth (Fig. S12). MODIS Chl-*a* indicated that the bloom persisted throughout February (Fig. S8). Haptophyte abundance in the sub-surface bloom at PS2 was lower than at the MPA (0.1 compared to 0.25 μg L^{-1} Chl-*a*) but higher than non-bloom Antarctic coastal regions (∼0.05 μg L^{-1} Chl-*a*) and haptophytes represented a higher proportion of total Chl-*a* (Fig. S12). The PS2 bloom had a higher abundance of dinoflagellates than the MPA (0.22 versus 0.07 μg L^{-1} Chl-*a*) as well as significantly lower fraction of diatoms compared to the MPA (0.3 compared to 2.5 μg L^{-1} Chl-*a*). Dissolved DMS/O/P concentrations were not available for this region. Potentially indicative of a more heterotrophic phase and downwelling at the shelf was the consistently higher pCO_2 (∼350 ppm) compared to the MPA (∼208 ppm), lower O_2 saturation (<100 %) (Fig. S9), and higher CDOM (2–3 ppb throughout the measured water column ∼0–200 m; Fig. S12), suggesting increased heterotrophy in the PS2 region (Fig. S9 and S12). A 1000 L sample of natural seawater was collected at PS2 in deckboard 2000 L mesocosm tanks and incubated over 10 days (Supplementary Information Text S5). The mesocosm headspace concentration of MeSH exhibited significant diel variability on the order of 10s of ppt with maxima in low light conditions; whereas DMS showed little diurnal variability with the most significant changes occurring on the order of days (Fig. S14), providing further evidence of the photo-inhibition effect with higher MeSH associated with low light conditions.

Heterotrophic dinoflagellates can also play a key role in phytoplankton herbivory in coastal Antarctic waters (Archer et al., 1996), and the higher abundance of dinoflagellates at PS2 (Fig. S12d) may have contributed to higher heterotrophy in this region. The lower proportion of diatoms and higher proportion of haptophytes to total Chl-*a* at PS2 compared to the MPA (Fig. S12) may be indicative of grazing by Antarctic krill, which are known to congregate near the Antarctic continental slope (Freer et al., 2025) and prefer large diatoms, leaving small cells such as haptophytes behind, either due to selective feeding or the inefficient filtering of small cells with the feeding apparatus (Heidemann et al., 2024). Krill grazing may have a large influence on ocean biogeochemistry through pathways such as sloppy feeding and the production of faecal pellets, with associated organic material subject to bacterial remineralisation (Cavan et al., 2019). Such processes have been shown to result in increased dissolved-phase DMSP (Kasamatsu et al., 2004), which is required for the demethylation/demethiolation pathway to proceed to MeSH production (Fig. 1; Hopkins et al. 2023). We therefore postulate that the heterotrophic characteristics at PS2 were conducive to enhanced MeSH production independent of chlorophyll biomass (Kiene et al., 1999; Hopkins et al., 2023), and may explain the increased MeSH atmospheric concentrations at PS2 compared to the MPA.

3.5.3 Subtropical Front Region (42–52° S)

The highest atmospheric MeSH concentrations (up to 252 ppt) were observed over subantarctic waters between ∼42–52° S along the northward I9S Transect bounded by the Subtropical Front (16–23 Feb 2024; Fig. 2). DMS was also elevated

https://doi.org/10.5194/egusphere-2026-1346
Preprint. Discussion started: 13 April 2026

in this region (up to 1.37 ppb) and closely coupled with MeSH (R^2 = 0.72) with a MeSH:DMS ratio of ∼0.15 (Fig. S15). Underway SST and salinity data showed a step change from <6° C at 51° S to >10° C at 49° S and salinity 33.9 to 34.3 PSU (Fig. S12). Depth profiles of salinity and temperature indicate a shallower MLD of ∼50 m formed between 46–35° S (Fig. S12). The air masses sampled in this region were predominantly from the WNW and were mostly classified as oceanic low productivity (Fig. 3). However, air mass back trajectories combined with MODIS cBLChl-*a* indicate air masses with the highest VMS concentrations passed over a wide band of biological productivity between 44–36 °S (Fig. S4). Underway surface Chl-*a* fluorescence was low (<1 μg Chl-*a* L^{-1}) until around 48° S where it increased up to 2 μg Chl-*a* L^{-1} at ∼43 ° S. Depth profiles showed pronounced fluorescence within the MLD at 50–35° S with a high abundance of haptophytes (20–50 % of total Chl-*a*; Fig. S11; Fig. S12) in subantarctic waters between 50–43° S.

Coccolithophores and *Phaeocystis* sp. are the dominant genus of haptophytes in this region and these strong DMS/P producers are considered to be major contributors to the elevated seawater and atmospheric DMS/P observed during summer and autumn in subantarctic waters (Curran et al., 1998; McTaggart et al., 1995; Keller et al., 1989; Nissen et al., 2018). Enhanced atmospheric VMS and higher MeSH:DMS ratios have previously been reported over a coccolithophore-rich bloom in the Southwest Pacific Ocean (Lawson et al., 2020). Conversely, cooler waters (<6° C) south of 50° S in this study were dominated by diatoms, which produce less DMSP (Fig. S11; Fig. S12). A range of environmental factors including temperature, light, MLD, nutrient availability (particularly diatom-limiting silicic acid), as well as zooplankton grazing, are key factors controlling haptophyte and diatom populations, and therefore VMS emissions, in this region (Oliver et al., 2023; Nissen et al., 2018). Similarly to the sea ice region described above, rapid changes in temperature, salinity, MLD and nutrient availability along the subtropical frontal region may have resulted in an upregulation of DMS/P production as a stress response within the haptophyte assemblages present. In addition, higher cloud and rainfall conditions in this sampling period (Fig. S13) may have limited photo-inhibition of bacterioplankton resulting in the higher atmospheric MeSH concentrations associated with air masses from this region. Given its large spatial extent, this frontal band of elevated biological activity, and higher MeSH:DMS ratios (∼0.15) compared to the Antarctic Ice-Edge (∼0.05), indicates that these latitudes of the Southern Ocean could be an important regional and global source not only for DMS but also MeSH.

In summary, the underlying biological and oceanographic conditions observed during the case studies of VMS enhancements presented here for the Ice-Edge (MPA, PS2) and the Open Ocean (42–52° S) demonstrate strong controls on the abundance and speciation of atmospheric VMS. In particular, haptophyte abundance appears to be a key biological driver of marine DMS/O/P production. Furthermore, we hypothesise that heterotrophic processes, such as zooplankton grazing and bacterial catabolism controlled the relative MeSH:DMS yields within the surface ocean.

Taken together, these regime-dependent responses between Antarctic Ice-Edge and Open Ocean regions demonstrate that empirical relationships between biogeochemical properties, VMS, and MeSH:DMS cannot be applied uniformly across the Southern Ocean. Instead, they underscore that Southern Ocean phytoplankton dynamics and associated sulfur cycling emerge from the interaction of multiple environmental drivers (temperature, light, and MLD across fronts), which organise distinct vertical biomass and community compositions in ice-edge versus offshore systems (Thomalla et al., 2023). In ice-edge regimes, intense, spatially coherent surface blooms under shallow stratification and episodic nutrient supply can link surface Chl-*a*

https://doi.org/10.5194/egusphere-2026-1346
Preprint. Discussion started: 13 April 2026

more directly to atmospheric VMS emissions; whereas in offshore regions, weaker, more deeply mixed, and spatially sparse biological activity decouples surface Chl-*a* from atmospheric VMS. Our results show that predictive frameworks for DMS and MeSH contributions to the total Southern Ocean VMS burden must be explicitly aware of regional differences in physical–biogeochemical regimes and the influence of air mass history.

3.6 First Generation Oxidative Fate of DMS

Once emitted into the atmosphere, gas-phase oxidation and multiphase chemical processing are important loss mechanisms for VMS (Fig. 1), which contribute to the atmospheric sulfur cycle and to Southern Ocean aerosol and cloud processes (Charlson et al., 1987; von Glasow and Crutzen, 2004; Carslaw et al., 2013). In the cloud-free marine boundary layer, DMS is oxidised to DMSO, mainly via oxidation by OH-addition and BrO (Fig. 1; Hoffmann et al. 2016). BrO oxidation has previously been identified as a potentially important mechanism, contributing up to 44 % of global DMSO production in a modeled global tropospheric DMSO budget (Chen et al., 2018). MeSH is primarily oxidized via H-abstraction to short-lived radicals and SO_2 (not measured on MISO), and apart from acting as an OH-scavenger, MeSH oxidation would not contribute to the observed atmospheric DMSO abundance (Novak et al., 2022; Wohl et al., 2024). Observed DMS and DMSO concentrations are well correlated at the Ice-Edge (R^2 = 0.69, $p < 0.01$) and weakly but still significantly correlated over the Open Ocean (R^2 = 0.04, $p < 0.01$). The DMSO:DMS ratio varied significantly (∼0–1) with temperature across spatial regions of the Southern Ocean (Fig. 6).

South of the atmospheric Polar Front, subzero air temperatures coincide with elevated DMSO:DMS and a strong coupling (R^2 = 0.69, Fig. 6), consistent with previous work highlighting temperature-driven partitioning of DMS oxidation products near Antarctica (Berresheim and Eisele, 1998; Davis et al., 1998; Legrand et al., 2001). We propose that the strong DMSO:DMS coupling at the Ice-Edge could be evidence of local, rapid OH-addition oxidation of DMS in the photochemically active boundary layer of the summertime Antarctic Ice-Edge. This pathway may be amplified by BrO-mediated oxidation, which has reaction rates an order of magnitude faster than OH-mediated oxidation in the Antarctic environment, leading to estimated DMS lifetimes on the order of minutes to hours (Saiz-Lopez et al., 2007; Mynard et al., 2025b; Davis et al., 1998) which is consistent with the observed DMSO:DMS correlation at the Ice-Edge (Fig. 6). The DMSO:DMS correlation is even stronger and an increased slope is observed (R^2 = 0.76, slope = 0.16, $p < 0.01$; Fig. S17) when only considering intense sunlight conditions (PAR >85th percentile: >700 μmol m^{-2} s^{-1}) and low-moderate *in-situ* wind speeds (1–10 ms^{-1}), suggesting that under such conditions local photochemical production of DMSO from DMS likely occurred at the Ice-Edge. This is further supported by the absence of any significant time lag in the time-varying behaviour of the two species. An autocorrelation analysis shows that they are optimally coupled at the time of measurement, with no improvement in the correlation when time-lagging the data (Fig. S18). Although these are likely significantly influenced by meteorology, the lack of observable lag under stable low wind speed conditions points to the importance of oxidation mechanisms, which occur faster than characterized reactions between DMS and OH. However, co-emission of DMSO and DMS from the surface ocean could, in theory, also explain the lack of lagged time varying behaviour.

https://doi.org/10.5194/egusphere-2026-1346
Preprint. Discussion started: 13 April 2026

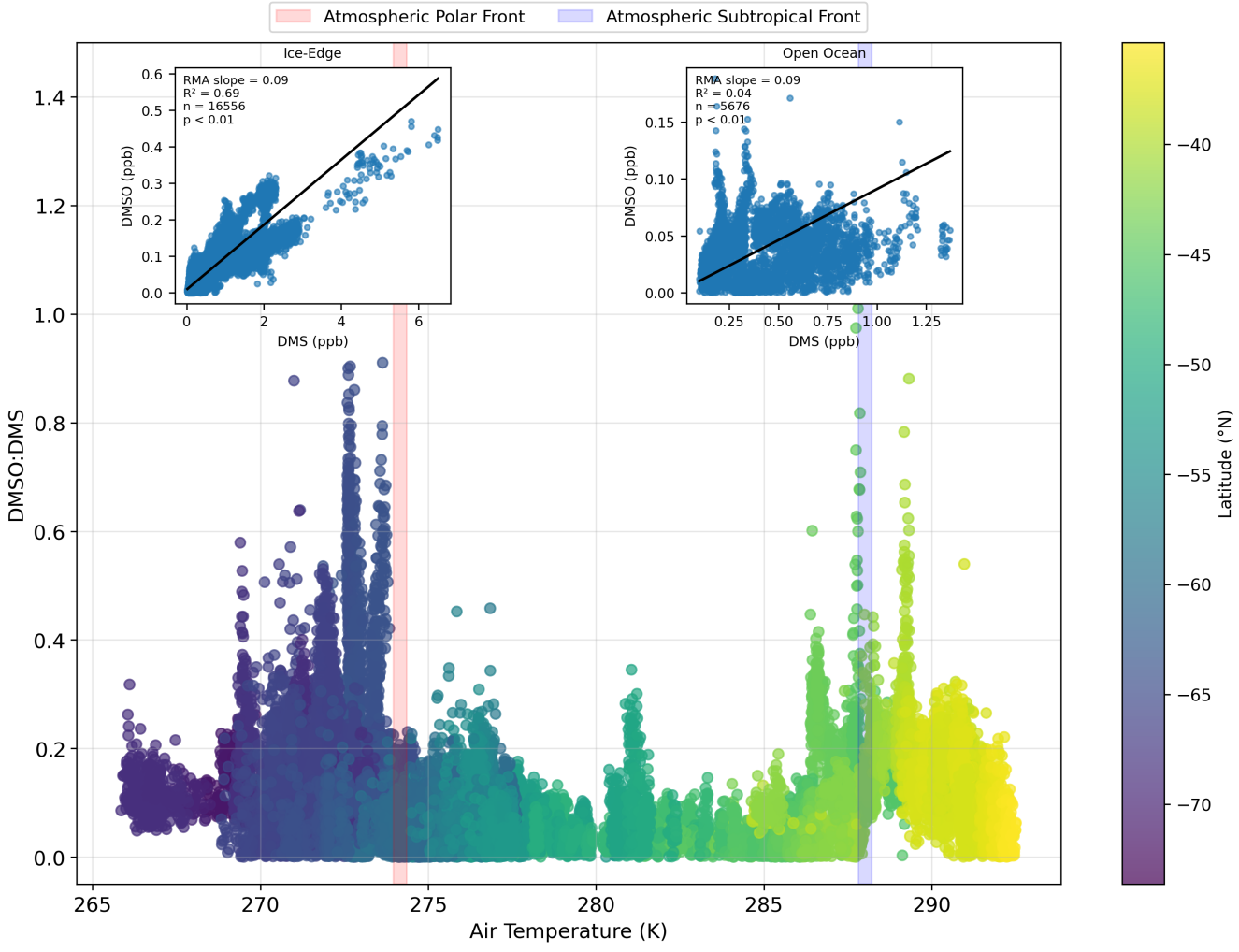

Figure 6. Atmospheric DMSO:DMS ratio across measured air temperatures. Latitudes south of the atmospheric Polar Front (<62° S, red highlight) are considered Ice-Edge with associated DMSO:DMS RMA scatter plot (top left), and north of the atmospheric Polar Front (>62° S) spanning the Southern Ocean and the atmospheric Subtropical Front (~40–50° S, blue highlight) are considered Open Ocean with associated DMSO:DMS RMA scatter plot (top right).

https://doi.org/10.5194/egusphere-2026-1346
Preprint. Discussion started: 13 April 2026

DMSO is highly soluble in seawater, with a Henry's law constant 5 orders of magnitude lower than that of DMS (Dacey et al., 1984; Watts and Brimblecombe, 1987). Its ventilation from seawater is therefore not thermodynamically favoured. This is supported by observations during on board mesocosm incubation experiments which were conducted along the Antarctic Ice-Edge (described in Supplementary Information Text S5). In these experiments, DMS concentrations reached as high as 15 ppb (∼2-3 times the median ambient concentrations) within the oxidant-free mesocosm headspace, while DMSO had a maximum atmospheric concentration of 40 ppt, it was rarely observed above detection limits in the headspace, and did not co-vary with DMS. This is also consistent with Kilgour et al. (2022) who studied an induced phytoplankton bloom and found little evidence for ventilation of DMS oxidation products into oxidant-free headspace environments. Therefore, multiple lines of evidence point to gas-phase production of DMSO from DMS oxidation pathways rather than ventilation from the ocean surface as the dominant source of DMSO.

However, in addition to microbial degradation and ventilation to the atmosphere, DMS is also lost from the surface ocean via photolysis (Galí et al., 2023). This process occurs in the upper mixed layer when DMS is oxidised by reactive species generated from light absorption by photo-active substances, particularly CDOM and nitrate, with peak photolysis at UV wavelengths ∼320–330 nm, yielding DMSO as the main product (Brimblecombe and Shooter, 1986; Galí et al., 2016). The mesocosm setup used in the experiments (Sect. 3.5; Fig. S12) filtered out UV wavelengths <364nm. Overall, DMS loss via photo-oxidation has been shown to be particularly important in the Southern Ocean (Galí et al., 2023) and potentially responsible for the decoupling observed between DMS and Chl-*a* in frontal regions exhibiting high CDOM and nitrate concentrations (McNabb and Tortell, 2023). It is unclear if DMSO produced at the air-sea interface can be efficiently transferred to the atmosphere; however, it may provide another possible explanation for the tight DMS:DMSO coupling observed in the DMS hotspots encountered along the Ice-Edge in this study.

We found no consistent correlation between any of the VMS species (DMS, MeSH, and DMSO) and any of the later VMS oxidation products measured during the MISO voyage, namely MSA (g), SA (g), or aerosol-phase sulfate (all $R^2 < 0.2$; see Fig. S6). This decoupling is likely indicative of the importance of multiphase chemistry, meteorology, and sinks in the atmospheric concentrations of later VMS oxidation products, and is consistent with other studies of atmospheric sulfur in remote marine atmospheres (Read et al., 2008; Zhang et al., 2024; Shen et al., 2022; Chen et al., 2012). Persistent low-pressure systems and cyclones around the Antarctic continent promote strong vertical uplift, shifting much of the MSA and SA production into the free-troposphere where low temperatures and low condensation sink favour slower, multistep oxidation pathways and new particle formation. Recent work by Miljevic et al. (2025) suggests that katabatic outflow transports free-tropospheric, highly acidic aerosol particles back into the boundary layer, where low RH and high acidity can drive evaporation of particle-phase MSA, which helps to explain the decoupling between our observed MSA/SA from local VMS emissions.

As illustrated in Fig. 6, the DMSO:DMS ratio is significantly and consistently higher under the cold conditions of the Ice-Edge below the atmospheric Polar Front (median DMSO:DMS = 12 %, Fig. 3) than in Open Ocean conditions between the polar and subtropical fronts (median DMSO:DMS = 5 %, Fig. 3). A significant potential contributor to this dynamic is likely the temperature dependence of DMS oxidative pathways, illustrated in Fig. 1. As described in Berresheim and Eisele (1998), at low temperatures (<285 K) the OH addition pathway is favoured, leading to higher production of DMSO and MSA. Under

https://doi.org/10.5194/egusphere-2026-1346
Preprint. Discussion started: 13 April 2026

warmer conditions however, the H-abstraction DMS oxidation pathway is more favoured, which would lead to lower yields of DMSO and higher yields of SO_2 and SA. While the transition from a low to high DMSO:DMS regime occurs at significantly less than 285 K and synoptic scale dynamics related to DMS lofting above the boundary layer have also been identified as important contributors to DMSO production (Nowak et al., 2001; Jourdain and Legrand, 2001), the temperature dependence of oxidative fate remains an important likely contributor to observed dynamics. As the air temperature increases north of the atmospheric Polar Front and over the Open Ocean, we find that DMSO:DMS generally decreases and they become decoupled (R^2 = 0.06, Fig. 6). This is consistent with austral summer DMSO measurements conducted at a similar latitude at Amsterdam Island (37.83° S, 77.50° E; Sciare et al. 2000), which found that DMSO co-varied with DMS but they were only moderately correlated (R^2 = 0.21). Our current temperature-dependent conceptual framework for VMS oxidation does not fully capture the observed behaviour of an increased DMSO:DMS ratio at the warmer Subtropical Front (42–52° S, Fig. 6). This suggests that latitudinal temperature gradients may not always be the primary factor responsible for DMSO:DMS variability across the broad regions of the Southern Ocean, although the mechanistic processes underlying this remain insufficiently understood and unresolved.

4 Conclusion

This study reveals that controls on atmospheric volatile methylated sulfur compounds (VMS) are highly regionally dependent, shaped by distinct biological regimes along the Antarctic Ice-Edge and by physical and meteorological drivers over the Open Ocean. At the Ice-Edge, extreme DMS episodes were tightly linked to recent ice-edge productivity, shallow mixed layers and high haptophyte contributions to total Chl-*a*, establishing monthly MODIS Chl-*a* coupled with modelled air mass back trajectories as a robust proxy for DMS source strength; but a poor proxy for MeSH, which was associated with heterotrophic activity and photo-physical conditions. Furthermore, DMS was a less reliable predictor of MeSH under these high productivity, heterogeneous Antarctic coastal conditions. Given the very low MeSH:DMS ratios observed at the ice-edge in this study (<3%), approaches that infer MeSH fluxes and atmospheric abundances by scaling from DMS climatologies, as implemented in recent models (Wohl et al., 2024; Tashmim et al., 2025; Jacob et al., 2026), are likely to substantially overestimate MeSH contributions over this Antarctic coastal region.

North of the Polar Front, where biological sources are weaker and more deeply mixed, VMS variability was governed primarily by physical ocean structure, boundary-layer dynamics, humidity, air temperature and oxidant availability. In the Open Ocean, the lack of a robust predictor indicates that atmospheric VMS variability reflects the integrated effects of heterogeneous source regions, transport, and atmospheric processing, rather than clearly identifiable source-related drivers like those observed at the highly biologically mediated Antarctic Ice-Edge. Consistent with this, relationships with individual physical variables (e.g., mixed layer depth and bathymetry) likely capture the indirect influence of large-scale circulation, rather than a mechanistic control on VMS production or emission. While DMS and DMSO were strongly coupled at the Antarctic Ice-Edge, later oxidation products (MSA and SA) were further decoupled from their VMS precursors, reflecting the dominant influence of temperature-dependent pathways and air mass history.

https://doi.org/10.5194/egusphere-2026-1346
Preprint. Discussion started: 13 April 2026

Together, these findings underscore that Antarctic VMS cannot be represented by biological proxies alone. Accurate prediction of sulfur emissions and their contribution to aerosol requires frameworks that couple ocean biogeochemistry with boundary-layer transport and temperature-dependent oxidation. While these are being rapidly introduced into Earth System Models, explicitly resolving all relevant processes in fully coupled biogeochemistry–ocean–atmosphere simulations currently remains computationally impractical on climate-relevant timescales (Bock et al., 2021; Bonan and Doney, 2018; Mallet et al., 2023b). Crucially, future changes in Southern Ocean stratification and circulation are likely to further destabilise empirical frameworks for predicting marine VMS production and emissions.

A targeted strategy for strengthening these frameworks would incorporate (i) developing higher-resolution, time-varying spatial maps of seawater VMS concentrations and air–sea fluxes to better constrain source strength and temporal variability, and (ii) improving representation of VMS chemical processing in atmospheric models, including DMS and MeSH and multiphase formation and partitioning of their oxidation products. Linking these observationally constrained emissions to expanded sulfur chemistry schemes would enable targeted sensitivity experiments that quantify how aerosol and cloud properties respond to key drivers over the Southern Ocean, providing a useful pathway to regime-aware parameterisations without requiring explicit inclusion of all underlying processes.

Data availability. The MISO PTR-ToF-MS dataset is publicly available via Mynard et al. (2025a). The MISO ToF-ACSM dataset is publicly available via Mynard et al. (2026). Moderate Resolution Imaging Spectroradiometer Aqua satellite retrievals are publicly available via (NASA Earth Observations, 2025). All RV *Investigator* MISO (IN2024_V01) underway data, Triaxus tows and CTD profiles are publicly available via CSIRO National Collections and Marine Infrastructure (2024). The ARMOR3D NRT–TSHUVMld Global Ocean Observation-based product is publicly available via https://doi.org/10.48670/moi-00052 (Buongiorno Nardelli, 2020).

Author contributions. Conceptualization: CM, EBF, RS, BM, MDM, RH, ED; Data curation: CM, KW, BJM, PDT, SM, AG; Formal analysis: CM, EBF, BJM, RS, AG, RH, ED; Investigation: CM, EBF, JA, BJM, RS, PDT, AQ, BM, MDM, RH, ED; Methodology: CM, EBF, JA, KW, BJM, RS, PDT, BM, MDM, RH, ED; Resources: KW, RS, PDT, AG, BM, MDM, RH, ED; Supervision: STS, AP, MDM, EBF, RH, ED; Visualization: CM; Writing - original draft: CM, EBF, ED; Writing - review and editing: JA, KW, BJM, RS, STS, AP, BM, MDM, RH.

Competing interests. The authors have no competing interests to declare.

Acknowledgements. The authors wish to acknowledge the support of the CSIRO Marine National Facility for providing sea time on the RV Investigator, along with assistance from support personnel, access to scientific equipment, and data management services. The MISO voyage research was funded through a grant of sea time on the RV Investigator CSIRO Marine National Facility (https://ror.org/01mae9353). The

https://doi.org/10.5194/egusphere-2026-1346
Preprint. Discussion started: 13 April 2026

MISO voyage campaign received grant funding from the Australian Government as part of the Antarctic Science Collaboration Initiative program, under the Australian Antarctic Program Partnership, ASCI000002.

https://doi.org/10.5194/egusphere-2026-1346
Preprint. Discussion started: 13 April 2026

References

Allan, J. D., Delia, A. E., Coe, H., Bower, K. N., Alfarra, M., Jimenez, J. L., Middlebrook, A. M., Drewnick, F., Onasch, T. B., Canagaratna, M. R., Jayne, J. T., and Worsnop, D. R.: A generalised method for the extraction of chemically resolved mass spectra from Aerodyne aerosol mass spectrometer data, Journal of Aerosol Science, 35, 909–922, https://doi.org/10.1016/j.jaerosci.2004.02.007, publisher: Elsevier Ltd, 2004.

Archer, S., Leakey, R., Burkill, P., and Sleigh, M.: Microbial dynamics in coastal waters of East Antarctica: herbivory by heterotrophic dinoflagellates, Marine Ecology Progress Series, 139, 239–255, https://doi.org/10.3354/meps139239, 1996.

Arnold, S. R., Spracklen, D. V., Gebhardt, S., Custer, T., Williams, J., Peeken, I., and Alvain, S.: Relationships between atmospheric organic compounds and air-mass exposure to marine biology, Environmental Chemistry, 7, 232–241, https://doi.org/10.1071/EN09144, 2010.

Asher, E. C., Dacey, J. W. H., Mills, M. M., Arrigo, K. R., and Tortell, P. D.: High concentrations and turnover rates of DMS, DMSP and DMSO in Antarctic sea ice, Geophysical Research Letters, 38, https://doi.org/10.1029/2011GL049712, _eprint: https://agupubs.onlinelibrary.wiley.com/doi/pdf/10.1029/2011GL049712, 2011.

Asher, E. C., Dacey, J. W. H., Jarniková, T., and Tortell, P. D.: Measurement of DMS, DMSO, and DMSP in natural waters by automated sequential chemical analysis, Limnology and Oceanography: Methods, 13, 451–462, https://doi.org/10.1002/lom3.10039, _eprint: https://aslopubs.onlinelibrary.wiley.com/doi/pdf/10.1002/lom3.10039, 2015.

Asher, E. C., Dacey, J. W. H., Stukel, M., Long, M. C., and Tortell, P. D.: Processes driving seasonal variability in DMS, DMSP, and DMSO concentrations and turnover in coastal Antarctic waters, Limnology and Oceanography, 62, 104–124, https://doi.org/10.1002/lno.10379, _eprint: https://onlinelibrary.wiley.com/doi/pdf/10.1002/lno.10379, 2017.

Bates, T. S., Lamb, B. K., Guenther, A., Dignon, J., and Stoiber, R. E.: Sulfur emissions to the atmosphere from natural sourees, Journal of Atmospheric Chemistry, 14, 315–337, https://doi.org/10.1007/BF00115242, publisher: Springer, 2004.

Berndt, T., Hoffmann, E. H., Tilgner, A., Stratmann, F., and Herrmann, H.: Direct sulfuric acid formation from the gas-phase oxidation of reduced-sulfur compounds, Nature Communications, 14, 4849, https://doi.org/10.1038/s41467-023-40586-2, publisher: Nature Publishing Group, 2023.

Berresheim, H.: Biogenic sulfur emissions from the Subantarctic and Antarctic Oceans, Journal of Geophysical Research: Atmospheres, 92, 13 245–13 262, https://doi.org/10.1029/JD092iD11p13245, _eprint: https://onlinelibrary.wiley.com/doi/pdf/10.1029/JD092iD11p13245, 1987.

Berresheim, H. and Eisele, F. L.: Sulfur Chemistry in the Antarctic Troposphere Experiment: An overview of project SCATE, Journal of Geophysical Research: Atmospheres, 103, 1619–1627, https://doi.org/10.1029/97JD00103, _eprint: https://onlinelibrary.wiley.com/doi/pdf/10.1029/97JD00103, 1998.

Bock, J., Michou, M., Nabat, P., Abe, M., Mulcahy, J. P., Olivié, D. J. L., Schwinger, J., Suntharalingam, P., Tjiputra, J., van Hulten, M., Watanabe, M., Yool, A., and Séférian, R.: Evaluation of ocean dimethylsulfide concentration and emission in CMIP6 models, Biogeosciences, 18, 3823–3860, https://doi.org/10.5194/bg-18-3823-2021, 2021.

Bonan, G. B. and Doney, S. C.: Climate, ecosystems, and planetary futures: The challenge to predict life in Earth system models, Science, 359, eaam8328, https://doi.org/10.1126/science.aam8328, 2018.

Breider, T. J., Chipperfield, M. P., Richards, N. a. D., Carslaw, K. S., Mann, G. W., and Spracklen, D. V.: Impact of BrO on dimethylsulfide in the remote marine boundary layer, Geophysical Research Letters, 37, https://doi.org/10.1029/2009GL040868, _eprint: https://agupubs.onlinelibrary.wiley.com/doi/pdf/10.1029/2009GL040868, 2010.

https://doi.org/10.5194/egusphere-2026-1346
Preprint. Discussion started: 13 April 2026

Brimblecombe, P. and Shooter, D.: Photo-oxidation of dimethylsulphide in aqueous solution, Marine Chemistry, 19, 343–353, https://doi.org/10.1016/0304-4203(86)90055-1, 1986.

Buongiorno Nardelli, B.: A multi-year time series of observation-based 3D horizontal and vertical quasi-geostrophic global ocean currents, Earth System Science Data, 12, 1711–1723, https://doi.org/10.5194/essd-12-1711-2020, 2020.

Carslaw, K. S., Lee, L. A., Reddington, C. L., Pringle, K. J., Rap, A., Forster, P. M., Mann, G. W., Spracklen, D. V., Woodhouse, M. T., Regayre, L. A., and Pierce, J. R.: Large contribution of natural aerosols to uncertainty in indirect forcing, Nature, 503, 67–71, https://doi.org/10.1038/nature12674, publisher: Nature Publishing Group, 2013.

Cavan, E. L., Belcher, A., Atkinson, A., Hill, S. L., Kawaguchi, S., McCormack, S., Meyer, B., Nicol, S., Ratnarajah, L., Schmidt, K., Steinberg, D. K., Tarling, G. A., and Boyd, P. W.: The importance of Antarctic krill in biogeochemical cycles, Nature Communications, 10, 4742, https://doi.org/10.1038/s41467-019-12668-7, 2019.

Charlson, R. J., Lovelock, J. E., Andreae, M. O., and Warren, S. G.: Oceanic phytoplankton, atmospheric sulphur, cloud albedo and climate, Nature, 326, 655–661, https://doi.org/10.1038/326655a0, publisher: Nature Publishing Group, 1987.

Chen, J., Lane, J. R., Bates, K. H., and Kjaergaard, H. G.: Atmospheric Gas-Phase Formation of Methanesulfonic Acid, Environmental Science & Technology, 57, 21 168–21 177, https://doi.org/10.1021/acs.est.3c07120, publisher: American Chemical Society, 2023.

Chen, L., Wang, J., Gao, Y., Xu, G., Yang, X., Lin, Q., and Zhang, Y.: Latitudinal distributions of atmospheric MSA and MSA/nss-SO42- ratios in summer over the high latitude regions of the Southern and Northern Hemispheres, Journal of Geophysical Research: Atmospheres, 117, https://doi.org/10.1029/2011JD016559, _eprint: https://agupubs.onlinelibrary.wiley.com/doi/pdf/10.1029/2011JD016559, 2012.

Chen, Q., Sherwen, T., Evans, M., and Alexander, B.: DMS oxidation and sulfur aerosol formation in the marine troposphere: a focus on reactive halogen and multiphase chemistry, Atmospheric Chemistry and Physics, 18, 13 617–13 637, https://doi.org/https://doi.org/10.5194/acp-18-13617-2018, 2018.

CSIRO National Collections and Marine Infrastructure: IN2024_V01 Southern Ocean Voyage Data [Dataset], https://www.cmar.csiro.au/data/trawler/survey_details.cfm?survey=IN2024_V01, 2024.

Curran, M. A. J., Jones, G. B., and Burton, H.: Spatial distribution of dimethylsulfide and dimethylsulfoniopropionate in the Australasian sector of the Southern Ocean, Journal of Geophysical Research: Atmospheres, 103, 16 677–16 689, https://doi.org/10.1029/97JD03453, _eprint: https://onlinelibrary.wiley.com/doi/pdf/10.1029/97JD03453, 1998.

Dacey, J. W. H., Wakeham, S. G., and Howes, B. L.: Henry's law constants for dimethylsulfide in freshwater and seawater, Geophysical Research Letters, 11, 991–994, https://doi.org/10.1029/GL011i010p00991, _eprint: https://agupubs.onlinelibrary.wiley.com/doi/pdf/10.1029/GL011i010p00991, 1984.

Davis, D., Chen, G., Kasibhatla, P., Jefferson, A., Tanner, D., Eisele, F., Lenschow, D., Neff, W., and Berresheim, H.: DMS oxidation in the Antarctic marine boundary layer: Comparison of model simulations and held observations of DMS, DMSO, DMSO2, H2SO4(g), MSA(g), and MSA(p), Journal of Geophysical Research: Atmospheres, 103, 1657–1678, https://doi.org/10.1029/97JD03452, _eprint: https://onlinelibrary.wiley.com/doi/pdf/10.1029/97JD03452, 1998.

Freer, J. J., Warwick-Evans, V., Skaret, G., Krafft, B. A., Fielding, S., and Trathan, P. N.: A new dynamic distribution model for Antarctic krill reveals interactions with their environment, predators, and the commercial fishery in the south Scotia Sea region, Limnology and Oceanography, 70, 833–849, https://doi.org/10.1002/lno.12809, _eprint: https://aslopubs.onlinelibrary.wiley.com/doi/pdf/10.1002/lno.12809, 2025.

Galí, M., Kieber, D. J., Romera-Castillo, C., Kinsey, J. D., Devred, E., Pérez, G. L., Westby, G. R., Marrasé, C., Babin, M., Levasseur, M., Duarte, C. M., Agustí, S., and Simó, R.: CDOM Sources and Photobleaching Control Quantum Yields for Oceanic DMS Photolysis, En-

https://doi.org/10.5194/egusphere-2026-1346
Preprint. Discussion started: 13 April 2026

vironmental Science & Technology, 50, 13 361–13 370, https://doi.org/10.1021/acs.est.6b04278, publisher: American Chemical Society, 2016.

Galí, M., Devred, E., Pérez, G. L., Kieber, D. J., and Simó, R.: Global Ocean dimethylsulfide photolysis rates quantified with a spectrally and vertically resolved model, Limnology and Oceanography Letters, 8, 760–769, https://doi.org/10.1002/lol2.10342, publisher: John Wiley & Sons, Ltd, 2023.

Goosse, H., Libera, S., Naveira Garabato, A. C., Richaud, B., Silvano, A., and Vancoppenolle, M.: Winter sea ice edge shaped by Antarctic Circumpolar Current pathways, The Cryosphere, 19, 5763–5779, https://doi.org/https://doi.org/10.5194/tc-19-5763-2025, 2025.

Halsey, K. H. and Giovannoni, S. J.: Biological controls on marine volatile organic compound emissions: A balancing act at the sea-air interface, Earth-Science Reviews, 240, 104 360, https://doi.org/10.1016/j.earscirev.2023.104360, 2023.

Hamilton, D. S., Lee, L. A., Pringle, K. J., Reddington, C. L., Spracklen, D. V., and Carslaw, K. S.: Occurrence of pristine aerosol environments on a polluted planet, Proceedings of the National Academy of Sciences of the United States of America, 111, 18 466–18 471, https://doi.org/10.1073/PNAS.1415440111, publisher: National Academy of Sciences, 2014.

Hayward, A., Pinkerton, M. H., and Gutierrez-Rodriguez, A.: phytoclass: A pigment-based chemotaxonomic method to determine the biomass of phytoplankton classes, Limnology and Oceanography: Methods, 21, 220–241, https://doi.org/10.1002/lom3.10541, _eprint: https://aslopubs.onlinelibrary.wiley.com/doi/pdf/10.1002/lom3.10541, 2023.

Hayward, A., Pinkerton, M. H., Wright, S. W., Gutiérrez-Rodriguez, A., and Law, C. S.: Twenty-six years of phytoplankton pigments reveal a circumpolar Class Divide around the Southern Ocean, Communications Earth & Environment, 5, 92, https://doi.org/10.1038/s43247-024-01261-6, publisher: Nature Publishing Group, 2024.

Hayward, A., Murray, T., Di Geronimo, S., Wright, S. W., Westwood, K., Aasim Khan, M., Gutiérrez-Rodríguez, A., and Pinkerton, M. H.: Phytoclass, Now with a GUI: Point-and-Click Pigment Chemotaxonomy, Limnology and Oceanography Bulletin, https://doi.org/10.1002/lob.70012, publisher: John Wiley & Sons, Ltd, 2026.

Heidemann, A. C., Westwood, K. J., Foppert, A., Wright, S. W., Klocker, A., Vives, C. R., Wotherspoon, S., and Bestley, S.: Drivers of phytoplankton distribution, abundance and community composition off East Antarctica, from 55-80°E (CCAMLR Division 58.4.2 East), Frontiers in Marine Science, 11, https://doi.org/10.3389/fmars.2024.1454421, 2024.

Hoffmann, E. H., Tilgner, A., Schrödner, R., Bräuer, P., Wolke, R., and Herrmann, H.: An advanced modeling study on the impacts and atmospheric implications of multiphase dimethyl sulfide chemistry, Proceedings of the National Academy of Sciences, 113, 11 776–11 781, https://doi.org/10.1073/pnas.1606320113, publisher: Proceedings of the National Academy of Sciences, 2016.

Hopkins, F. E., Archer, S. D., Bell, T. G., Suntharalingam, P., and Todd, J. D.: The biogeochemistry of marine dimethylsulfide, Nature Reviews Earth & Environment 2023 4:6, 4, 361–376, https://doi.org/10.1038/s43017-023-00428-7, publisher: Nature Publishing Group, 2023.

Hufford, G. E., McCartney, M. S., and Donohue, K. A.: Northern boundary currents and adjacent recirculations off southwestern Australia, Geophysical Research Letters, 24, 2797–2800, https://doi.org/10.1029/97GL02278, _eprint: https://onlinelibrary.wiley.com/doi/pdf/10.1029/97GL02278, 1997.

Hulswar, S., Simó, R., Galí, M., Bell, T. G., Lana, A., Inamdar, S., Halloran, P. R., Manville, G., and Mahajan, A. S.: Third revision of the global surface seawater dimethyl sulfide climatology (DMS-Rev3), Earth System Science Data, 14, 2963–2987, https://doi.org/10.5194/essd-14-2963-2022, publisher: Copernicus GmbH, 2022.

https://doi.org/10.5194/egusphere-2026-1346
Preprint. Discussion started: 13 April 2026

Humphries, R., Keywood, M., Gribben, S., McRobert, I., Ward, J., Selleck, P., Taylor, S., Harnwell, J., Flynn, C., Kulkarni, G., Mace, G., Protat, A., Alexander, S., and McFarquhar, G.: Southern Ocean latitudinal gradients of Cloud Condensation Nuclei, Atmospheric Chemistry and Physics, 21, 12 757–12 782, https://doi.org/https://doi.org/10.5194/acp-21-12757-2021, 2021.

Humphries, R. S., McRobert, I. M., Ponsonby, W. A., Ward, J. P., Keywood, M. D., Loh, Z. M., Krummel, P. B., and Harnwell, J.: Identification of platform exhaust on the RV Investigator, Atmospheric Measurement Techniques, 12, 3019–3038, https://doi.org/10.5194/amt-12-3019-2019, 2019.

Ishino, S., Willis, M. D., Angot, H., Bartels-Rausch, T., Crabeck, O., Delille, B., Dunne, E., Franklin, E., Haddon, A., Hayashida, H., Joge, S. D., Lapere, R., Lim, H.-G., Mahajan, A. S., Mallet, M. D., Manville, G., Marelle, L., Nomura, D., Pratt, K. A., Peeken, I., Price, R., Simó, R., Stefels, J., Thomas, J. L., Zang, C. L., and Steiner, N.: The biogenic sulfur cycle in the coupled ocean–sea ice–atmosphere system, Elementa: Science of the Anthropocene, 14, 1–60, https://doi.org/10.1525/elementa.2025.00067, 2026.

Jacob, L. S. D., Harvey, B. E. H., Giorio, C., and Archibald, A. T.: Determining the key sources of uncertainty in dimethyl sulfide and methanethiol oxidation under tropical, temperate, and polar marine conditions, Atmospheric Chemistry and Physics, 26, 3567–3587, https://doi.org/10.5194/acp-26-3567-2026, 2026.

Jang, E., Park, K.-T., Yoon, Y. J., Kim, K., Gim, Y., Chung, H. Y., Lee, K., Choi, J., Park, J., Park, S.-J., Koo, J.-H., Fernandez, R. P., and Saiz-Lopez, A.: First-year sea ice leads to an increase in dimethyl sulfide-induced particle formation in the Antarctic Peninsula, Science of The Total Environment, 803, 150 002, https://doi.org/10.1016/j.scitotenv.2021.150002, 2022.

Jarníková, T. and Tortell, P. D.: Towards a revised climatology of summertime dimethylsulfide concentrations and sea–air fluxes in the Southern Ocean, Environmental Chemistry, 13, 364–378, https://doi.org/https://doi.org/10.1071/EN14272, 2016.

Jourdain, B. and Legrand, M.: Seasonal variations of atmospheric dimethylsulfide, dimethylsulfoxide, sulfur dioxide, methanesulfonate, and non-sea-salt sulfate aerosols at Dumont d'Urville (coastal Antarctica) (December 1998 to July 1999), Journal of Geophysical Research: Atmospheres, 106, 14 391–14 408, https://doi.org/10.1029/2000JD900841, _eprint: https://agupubs.onlinelibrary.wiley.com/doi/pdf/10.1029/2000JD900841, 2001.

Kasamatsu, N., Kawaguchi, S., Watanabe, S., Odate, T., and Fukuchi, M.: Possible impacts of zooplankton grazing on dimethylsulfide production in the Antarctic Ocean, Canadian Journal of Fisheries and Aquatic Sciences, 61, 736–743, https://doi.org/10.1139/f04-072, publisher: NRC Research Press, 2004.

Keller, M. D., Bellows, W. K., and Guillard, R. R. L.: Dimethyl Sulfide Production in Marine Phytoplankton, in: Biogenic Sulfur in the Environment, vol. 393 of *ACS Symposium Series*, pp. 167–182, American Chemical Society, https://doi.org/10.1021/bk-1989-0393.ch011, section: 11, 1989.

Kettle, A. J., Andreae, M. O., Amouroux, D., Andreae, T. W., Bates, T. S., Berresheim, H., Bingemer, H., Boniforti, R., Curran, M. a. J., DiTullio, G. R., Helas, G., Jones, G. B., Keller, M. D., Kiene, R. P., Leck, C., Levasseur, M., Malin, G., Maspero, M., Matrai, P., McTaggart, A. R., Mihalopoulos, N., Nguyen, B. C., Novo, A., Putaud, J. P., Rapsomanikis, S., Roberts, G., Schebeske, G., Sharma, S., Simó, R., Staubes, R., Turner, S., and Uher, G.: A global database of sea surface dimethylsulfide (DMS) measurements and a procedure to predict sea surface DMS as a function of latitude, longitude, and month, Global Biogeochemical Cycles, 13, 399–444, https://doi.org/10.1029/1999GB900004, _eprint: https://onlinelibrary.wiley.com/doi/pdf/10.1029/1999GB900004, 1999.

Kiene, R. P., Linn, L. J., González, J., Moran, M. A., and Bruton, J. A.: Dimethylsulfoniopropionate and methanethiol are important precursors of methionine and protein-sulfur in marine bacterioplankton, Applied and Environmental Microbiology, 65, 4549–4558, https://doi.org/10.1128/AEM.65.10.4549-4558.1999, 1999.

https://doi.org/10.5194/egusphere-2026-1346
Preprint. Discussion started: 13 April 2026

Kilgour, D. B., Novak, G. A., Sauer, J. S., Moore, A. N., Dinasquet, J., Amiri, S., Franklin, E. B., Mayer, K., Winter, M., Morris, C. K., Price, T., Malfatti, F., Crocker, D. R., Lee, C., Cappa, C. D., Goldstein, A. H., Prather, K. A., and Bertram, T. H.: Marine gas-phase sulfur emissions during an induced phytoplankton bloom, Atmospheric Chemistry and Physics, 22, 1601–1613, https://doi.org/10.5194/acp-22-1601-2022, 2022.

Kilgour, D. B., Jernigan, C. M., Garmash, O., Aggarwal, S., Zhou, S., Mohr, C., Salter, M. E., Thornton, J. A., Wang, J., Zieger, P., and Bertram, T. H.: Cloud processing of dimethyl sulfide (DMS) oxidation products limits sulfur dioxide (SO_2) and carbonyl sulfide (OCS) production in the eastern North Atlantic marine boundary layer, Atmospheric Chemistry and Physics, 25, 1931–1947, https://doi.org/10.5194/acp-25-1931-2025, publisher: Copernicus GmbH, 2025.

Kirst, G. O., Thiel, C., Wolff, H., Nothnagel, J., Wanzek, M., and Ulmke, R.: Dimethylsulfoniopropionate (DMSP) in icealgae and its possible biological role, Marine Chemistry, 35, 381–388, https://doi.org/10.1016/S0304-4203(09)90030-5, 1991.

Koga, S., Nomura, D., and Wada, M.: Variation of dimethylsulfide mixing ratio over the Southern Ocean from 36°S to 70°S, Polar Science, 8, 306–313, https://doi.org/10.1016/j.polar.2014.04.002, 2014.

Lana, A., Bell, T. G., Simó, R., Vallina, S. M., Ballabrera-Poy, J., Kettle, A. J., Dachs, J., Bopp, L., Saltzman, E. S., Stefels, J., Johnson, J. E., and Liss, P. S.: An updated climatology of surface dimethlysulfide concentrations and emission fluxes in the global ocean, Global Biogeochemical Cycles, 25, https://doi.org/10.1029/2010GB003850, _eprint: https://onlinelibrary.wiley.com/doi/pdf/10.1029/2010GB003850, 2011.

Lawson, S. J., Law, C. S., Harvey, M. J., Bell, T. G., Walker, C. F., De Bruyn, W. J., and Saltzman, E. S.: Methanethiol, dimethyl sulfide and acetone over biologically productive waters in the southwest Pacific Ocean, Atmospheric Chemistry and Physics, 20, 3061–3078, https://doi.org/10.5194/acp-20-3061-2020, publisher: Copernicus GmbH, 2020.

Legrand, M., Sciare, J., Jourdain, B., and Genthon, C.: Subdaily variations of atmospheric dimethylsulfide, dimethylsulfoxide, methanesulfonate, and non-sea-salt sulfate aerosols in the atmospheric boundary layer at Dumont d'Urville (coastal Antarctica) during summer, Journal of Geophysical Research: Atmospheres, 106, 14 409–14 422, https://doi.org/10.1029/2000JD900840, _eprint: https://onlinelibrary.wiley.com/doi/pdf/10.1029/2000JD900840, 2001.

Levasseur, M., Gosselin, M., and Michaud, S.: A new source of dimethylsulfide (DMS) for the arctic atmosphere: ice diatoms, Marine Biology, 121, 381–387, https://doi.org/10.1007/BF00346748, publisher: Springer, 1994.

Mallet, M., Protat, A., Mace, G., Alroe, J., Barber, K., Alexander, S., Franklin, E., Bekemeier, C., Chambers, S., Crawford, H., Creamean, J., Dunne, E., Foppart, A., Griffiths, A., Harnwell, J., Humphries, R., Meyerink, S., Miljevic, B., Molloy, S., Mynard, C., Powell, J., Rintoul, S., Sodano, S., Taylor, S., Ward, J., Williams, A., and Winton, H.: Atmospheric observations from the MISO (Multidisciplinary Investigations of the Southern Ocean) voyage [in prep], 2026.

Mallet, M. D., Alexander, S. P., Protat, A., and Fiddes, S. L.: Reducing Southern Ocean Shortwave Radiation Errors in the ERA5 Reanalysis with Machine Learning and 25 Years of Surface Observations, Artificial Intelligence for the Earth Systems, 2, e220 044, https://doi.org/10.1175/AIES-D-22-0044.1, section: Artificial Intelligence for the Earth Systems, 2023a.

Mallet, M. D., Humphries, R. S., Fiddes, S. L., Alexander, S. P., Altieri, K., Angot, H., Anilkumar, N., Bartels-Rausch, T., Creamean, J., Dall'Osto, M., Dommergue, A., Frey, M., Henning, S., Lannuzel, D., Lapere, R., Mace, G. G., Mahajan, A. S., McFarquhar, G. M., Meiners, K. M., Miljevic, B., Peeken, I., Protat, A., Schmale, J., Steiner, N., Sellegri, K., Simó, R., Thomas, J. L., Willis, M. D., Winton, V. H. L., and Woodhouse, M. T.: Untangling the influence of Antarctic and Southern Ocean life on clouds, Elementa: Science of the Anthropocene, 11, 00 130, https://doi.org/10.1525/elementa.2022.00130, 2023b.

https://doi.org/10.5194/egusphere-2026-1346
Preprint. Discussion started: 13 April 2026

Mallet, M. D., Miljevic, B., Humphries, R. S., Mace, G. G., Alexander, S. P., Protat, A., Chambers, S., Cravigan, L., DeMott, P. J., Fiddes, S., Harnwell, J., Keywood, M. D., McFarquhar, G. M., McRobert, I., Moore, K. A., Mynard, C., Osuagwu, C. G., Ristovski, Z., Selleck, P., Taylor, S., Ward, J., and Williams, A.: Biological enhancement of cloud droplet concentrations observed off East Antarctica, npj Climate and Atmospheric Science, 8, 1–7, https://doi.org/10.1038/s41612-025-00990-5, publisher: Nature Publishing Group, 2025.

Manville, G., Bell, T. G., Mulcahy, J. P., Simó, R., Galí, M., Mahajan, A. S., Hulswar, S., and Halloran, P. R.: Global analysis of the controls on seawater dimethylsulfide spatial variability, Biogeosciences, 20, 1813–1828, https://doi.org/https://doi.org/10.5194/bg-20-1813-2023, 2023.

Marine National Facility: MNF Voyage Highlights and Summary (MISO), Tech. rep., https://www.marine.csiro.au/data/reporting/get_file.cfm?eov_pub_id=3538, 2024.

McCartney, M. S. and Donohue, K. A.: A deep cyclonic gyre in the Australian–Antarctic Basin, Progress in Oceanography, 75, 675–750, https://doi.org/10.1016/j.pocean.2007.02.008, 2007.

McCulloch, R. and Tortell, P.: The determination of dimethyl sulfoxide in natural waters using electrochemical reduction, Limnology and Oceanography: Methods, 21, 529–541, https://doi.org/10.1002/lom3.10562, _eprint: https://aslopubs.onlinelibrary.wiley.com/doi/pdf/10.1002/lom3.10562, 2023.

McNabb, B. J. and Tortell, P. D.: Oceanographic controls on Southern Ocean dimethyl sulfide distributions revealed by machine learning algorithms, Limnology and Oceanography, 68, 616–630, https://doi.org/10.1002/lno.12298, 2023.

McNabb, B. J. and Tortell, P. D.: A potential photo-protective, antioxidant function for DMSO in marine phytoplankton, PLoS ONE, 20, e0317 951, https://doi.org/10.1371/journal.pone.0317951, 2025.

McTaggart, A. R., Burton, H. R., and Nguyen, B. C.: Emission and flux of DMS from the Australian Antarctic and Subantarctic Oceans during the 1988/89 summer, Journal of Atmospheric Chemistry, 20, 59–69, https://doi.org/10.1007/BF01099918, publisher: Springer, 1995.

Miljevic, B., Mallet, M. D., Osuagwu, C. G., Ristovski, Z. D., Humphries, R. S., Selleck, P., Taylor, S., and Keywood, M. D.: Aerosol acidity controls methanesulfonic acid evaporation from aerosols during Antarctic katabatic outflow, Communications Earth & Environment, 6, 1057, https://doi.org/10.1038/s43247-025-03041-2, publisher: Nature Publishing Group, 2025.

Mynard, C., Dunne, E., Franklin, E., Humphries, R., Harnwell, J., Mallet, M., and Alroe, J.: MISO - Atmospheric dimethyl sulfide (DMS) and methanethiol (MeSH) measurements from the RV Investigator voyage IN2024_V01, v1 [Dataset], https://doi.org/https://doi.org/10.25919/p8bz-p724, 2025a.

Mynard, C., Franklin, E. B., Alroe, J., Somerville, N., Patti, A., Siems, S. T., Williams, A., Mallet, M. D., Humphries, R., and Dunne, E.: Constraining Atmospheric Methanethiol Estimates Over the Southern Ocean, Geophysical Research Letters, 52, e2025GL116 470, https://doi.org/10.1029/2025GL116470, _eprint: https://agupubs.onlinelibrary.wiley.com/doi/pdf/10.1029/2025GL116470, 2025b.

Mynard, C., Humphries, R., Mallet, M., Alroe, J., Dunne, E., Franklin, E., and Harnwell, J.: MISO - Real-time aerosol chemistry measurements (ToF-ACSM) from the RV Investigator voyage IN2024_V01, v1 [Dataset], https://doi.org/10.25919/nk8s-0k87, 2026.

Müller, M., Mikoviny, T., Jud, W., D'Anna, B., and Wisthaler, A.: A new software tool for the analysis of high resolution PTR-TOF mass spectra, Chemometrics and Intelligent Laboratory Systems, 127, 158–165, https://doi.org/10.1016/J.CHEMOLAB.2013.06.011, publisher: Elsevier, 2013.

Nagahata, T., Kajiwara, H., Ohira, S.-I., and Toda, K.: Simple Field Device for Measurement of Dimethyl Sulfide and Dimethylsulfoniopropionate in Natural Waters, Based on Vapor Generation and Chemiluminescence Detection, Analytical Chemistry, 85, 4461–4467, https://doi.org/10.1021/ac303803w, publisher: American Chemical Society, 2013.

https://doi.org/10.5194/egusphere-2026-1346
Preprint. Discussion started: 13 April 2026

NASA Earth Observations: Chlorophyll Concentration (1 month - Aqua/MODIS) | NASA [Dataset], https://neo.gsfc.nasa.gov/view.php?datasetId=MY1DMM_CHLORA&date=2024-01-17, publisher: NASA Earth Observations (NEO), 2025.

Nissen, C., Vogt, M., Münnich, M., Gruber, N., and Haumann, F. A.: Factors controlling coccolithophore biogeography in the Southern Ocean, Biogeosciences, 15, 6997–7024, https://doi.org/https://doi.org/10.5194/bg-15-6997-2018, 2018.

Novak, G. A., Kilgour, D. B., Jernigan, C. M., Vermeuel, M. P., and Bertram, T. H.: Oceanic emissions of dimethyl sulfide and methanethiol and their contribution to sulfur dioxide production in the marine atmosphere, Atmospheric Chemistry and Physics, 22, 6309–6325, https://doi.org/10.5194/acp-22-6309-2022, publisher: Copernicus GmbH, 2022.

Nowak, J. B., Davis, D. D., Chen, G., Eisele, F. L., Mauldin III, R. L., Tanner, D. J., Cantrell, C., Kosciuch, E., Bandy, A., Thornton, D., and Clarke, A.: Airborne observations of DMSO, DMS, and OH at marine tropical latitudes, Geophysical Research Letters, 28, 2201–2204, https://doi.org/10.1029/2000GL012297, _eprint: https://agupubs.onlinelibrary.wiley.com/doi/pdf/10.1029/2000GL012297, 2001.

Oliver, H., McGillicuddy Jr., D. J., Krumhardt, K. M., Long, M. C., Bates, N. R., Bowler, B. C., Drapeau, D. T., and Balch, W. M.: Environmental Drivers of Coccolithophore Growth in the Pacific Sector of the Southern Ocean, Global Biogeochemical Cycles, 37, e2023GB007 751, https://doi.org/10.1029/2023GB007751, _eprint: https://agupubs.onlinelibrary.wiley.com/doi/pdf/10.1029/2023GB007751, 2023.

Piontek, J., Galgani, L., Nöthig, E.-M., Peeken, I., and Engel, A.: Organic matter composition and heterotrophic bacterial activity at declining summer sea ice in the central Arctic Ocean, Limnology and Oceanography, 66, S343–S362, https://doi.org/10.1002/lno.11639, _eprint: https://aslopubs.onlinelibrary.wiley.com/doi/pdf/10.1002/lno.11639, 2021.

Quinn, P. K. and Bates, T. S.: The case against climate regulation via oceanic phytoplankton sulphur emissions, Nature, 480, 51–56, https://doi.org/10.1038/nature10580, publisher: Nature Publishing Group, 2011.

Read, K. A., Lewis, A. C., Bauguitte, S., Rankin, A. M., Salmon, R. A., Wolff, E. W., Saiz-Lopez, A., Bloss, W. J., Heard, D. E., Lee, J. D., and Plane, J. M. C.: DMS and MSA measurements in the Antarctic Boundary Layer: impact of BrO on MSA production, Atmospheric Chemistry and Physics, 8, 2985–2997, https://doi.org/https://doi.org/10.5194/acp-8-2985-2008, 2008.

Rocco, M., Dunne, E., Salignat, R., Saint-Macary, A., Peltola, M., Barthelmeß, T., Chamba, G., Barr, N., Safi, K., Marriner, A., Deppeler, S., Rose, C., Uitz, J., Harnwell, J., Engel, A., Colomb, A., Saiz-Lopez, A., Harvey, M. J., Law, C. S., and Sellegri, K.: Relating Dimethyl Sulphide and Methanethiol Fluxes to Surface Biota in the South-West Pacific Using Shipboard Air-Sea Interface Tanks, Journal of Geophysical Research: Atmospheres, 130, e2024JD041 072, https://doi.org/10.1029/2024JD041072, _eprint: https://onlinelibrary.wiley.com/doi/pdf/10.1029/2024JD041072, 2025.

Saiz-Lopez, A., Mahajan, A. S., Salmon, R. A., Bauguitte, S. J.-B., Jones, A. E., Roscoe, H. K., and Plane, J. M. C.: Boundary Layer Halogens in Coastal Antarctica, Science, 317, 348–351, https://doi.org/10.1126/science.1141408, publisher: American Association for the Advancement of Science, 2007.

Schmale, J., Baccarini, A., Thurnherr, I., Henning, S., Efraim, A., Regayre, L., Bolas, C., Hartmann, M., Welti, A., Lehtipalo, K., Aemisegger, F., Tatzelt, C., Landwehr, S., Modini, R. L., Tummon, F., Johnson, J. S., Harris, N., Schnaiter, M., Toffoli, A., Derkani, M., Bukowiecki, N., Stratmann, F., Dommen, J., Baltensperger, U., Wernli, H., Rosenfeld, D., Gysel-Beer, M., and Carslaw, K. S.: Overview of the Antarctic Circumnavigation Expedition: Study of Preindustrial-like Aerosols and Their Climate Effects (ACE-SPACE), Bulletin of the American Meteorological Society, 100, 2260–2283, https://doi.org/10.1175/BAMS-D-18-0187.1, publisher: American Meteorological Society, 2019.

https://doi.org/10.5194/egusphere-2026-1346
Preprint. Discussion started: 13 April 2026

Sciare, J., Kanakidou, M., and Mihalopoulos, N.: Diurnal and seasonal variation of atmospheric dimethylsulfoxide at Amsterdam Island in the southern Indian Ocean, Journal of Geophysical Research: Atmospheres, 105, 17 257–17 265, https://doi.org/10.1029/1999JD901186, _eprint: https://agupubs.onlinelibrary.wiley.com/doi/pdf/10.1029/1999JD901186, 2000.

Shadwick, E. H., Rintoul, S. R., Tilbrook, B., Williams, G. D., Young, N., Fraser, A. D., Marchant, H., Smith, J., and Tamura, T.: Glacier tongue calving reduced dense water formation and enhanced carbon uptake, Geophysical Research Letters, 40, 904–909, https://doi.org/10.1002/grl.50178, _eprint: https://agupubs.onlinelibrary.wiley.com/doi/pdf/10.1002/grl.50178, 2013.

Shadwick, E. H., Tilbrook, B., and Currie, K. I.: Late-summer biogeochemistry in the Mertz Polynya: East Antarctica, Journal of Geophysical Research: Oceans, 122, 7380–7394, https://doi.org/10.1002/2017JC013015, _eprint: https://agupubs.onlinelibrary.wiley.com/doi/pdf/10.1002/2017JC013015, 2017.

Sheehan, C. E. and Petrou, K.: Dimethylated sulfur production in batch cultures of Southern Ocean phytoplankton, Biogeochemistry, 147, 53–69, https://doi.org/10.1007/s10533-019-00628-8, publisher: Springer, 2019.

Shen, J., Scholz, W., He, X.-C., Zhou, P., Marie, G., Wang, M., Marten, R., Surdu, M., Rörup, B., Baalbaki, R., Amorim, A., Ataei, F., Bell, D. M., Bertozzi, B., Brasseur, Z., Caudillo, L., Chen, D., Chu, B., Dada, L., Duplissy, J., Finkenzeller, H., Granzin, M., Guida, R., Heinritzi, M., Hofbauer, V., Iyer, S., Kemppainen, D., Kong, W., Krechmer, J. E., Kürten, A., Lamkaddam, H., Lee, C. P., Lopez, B., Mahfouz, N. G. A., Manninen, H. E., Massabò, D., Mauldin, R. L., Mentler, B., Müller, T., Pfeifer, J., Philippov, M., Piedehierro, A. A., Roldin, P., Schobesberger, S., Simon, M., Stolzenburg, D., Tham, Y. J., Tomé, A., Umo, N. S., Wang, D., Wang, Y., Weber, S. K., Welti, A., Wollesen de Jonge, R., Wu, Y., Zauner-Wieczorek, M., Zust, F., Baltensperger, U., Curtius, J., Flagan, R. C., Hansel, A., Möhler, O., Petäjä, T., Volkamer, R., Kulmala, M., Lehtipalo, K., Rissanen, M., Kirkby, J., El-Haddad, I., Bianchi, F., Sipilä, M., Donahue, N. M., and Worsnop, D. R.: High Gas-Phase Methanesulfonic Acid Production in the OH-Initiated Oxidation of Dimethyl Sulfide at Low Temperatures, Environmental Science & Technology, 56, 13 931–13 944, https://doi.org/10.1021/acs.est.2c05154, publisher: American Chemical Society, 2022.

Simó, R.: Production of atmospheric sulfur by oceanic plankton: biogeochemical, ecological and evolutionary links, Trends in Ecology & Evolution, 16, 287–294, https://doi.org/10.1016/S0169-5347(01)02152-8, 2001.

Simó, R. and Dachs, J.: Global ocean emission of dimethylsulfide predicted from biogeophysical data, Global Biogeochemical Cycles, 16, 26–1–26–10, https://doi.org/10.1029/2001GB001829, _eprint: https://agupubs.onlinelibrary.wiley.com/doi/pdf/10.1029/2001GB001829, 2002.

Simó, R. and Pedrós-Alió, C.: Role of vertical mixing in controlling the oceanic production of dimethyl sulphide, Nature, 402, 396–399, https://doi.org/10.1038/46516, publisher: Nature Publishing Group, 1999.

Simó, R., Hatton*, A. D., Malin, G., and Liss, P. S.: Particulate dimethyl sulphoxide in seawater: production by microplankton, Marine Ecology Progress Series, https://doi.org/10.3354/meps167291, 1998.

Simó, R., Pedrós-Alió, C., Malin, G., and Grimalt, J. O.: Biological turnover of DMS, DMSP and DMSO in contrasting open-sea waters, Marine Ecology Progress Series, https://doi.org/10.3354/meps203001, 2000.

Sokolov, S. and Rintoul, S. R.: On the relationship between fronts of the Antarctic Circumpolar Current and surface chlorophyll concentrations in the Southern Ocean, Journal of Geophysical Research: Oceans, 112, https://doi.org/10.1029/2006JC004072, _eprint: https://agupubs.onlinelibrary.wiley.com/doi/pdf/10.1029/2006JC004072, 2007.

Spiese, C. E., Kieber, D. J., Nomura, C. T., and Kiene, R. P.: Reduction of dimethylsulfoxide to dimethylsulfide by marine phytoplankton, Limnology and Oceanography, 54, 560–570, https://doi.org/10.4319/lo.2009.54.2.0560, _eprint: https://aslopubs.onlinelibrary.wiley.com/doi/pdf/10.4319/lo.2009.54.2.0560, 2009.

https://doi.org/10.5194/egusphere-2026-1346
Preprint. Discussion started: 13 April 2026

Sprenger, M. and Wernli, H.: GMD - The LAGRANTO Lagrangian analysis tool – version 2.0, Geoscientific Model Development, 8, 2569–2586, https://doi.org/doi:10.5194/gmd-8-2569-2015, 2015.

Stefels, J. and van Boekel, W.: Production of DMS from dissolved DMSP in axenic cultures of the marine phytoplankton species Phaeocystis sp., Marine Ecology Progress Series, 97, 11–18, https://doi.org/10.3354/meps097011, 1993.

Stefels, J., van Leeuwe, M. A., Jones, E. M., Meredith, M. P., Venables, H. J., Webb, A. L., and Henley, S. F.: Impact of sea-ice melt on dimethyl sulfide (sulfoniopropionate) inventories in surface waters of Marguerite Bay, West Antarctic Peninsula, Philosophical Transactions of the Royal Society A: Mathematical, Physical and Engineering Sciences, 376, 20170 169, https://doi.org/10.1098/rsta.2017.0169, publisher: Royal Society, 2018.

Sun, J., Todd, J. D., Thrash, J. C., Qian, Y., Qian, M. C., Temperton, B., Guo, J., Fowler, E. K., Aldrich, J. T., Nicora, C. D., Lipton, M. S., Smith, R. D., De Leenheer, P., Payne, S. H., Johnston, A. W., Davie-Martin, C. L., Halsey, K. H., and Giovannoni, S. J.: The abundant marine bacterium Pelagibacter simultaneously catabolizes dimethylsulfoniopropionate to the gases dimethyl sulfide and methanethiol, Nature Microbiology, 1, 16 065, https://doi.org/10.1038/NMICROBIOL.2016.65, publisher: Nature Publishing Group, 2016.

Taalba, A., Xie, H., Scarratt, M. G., Bélanger, S., and Levasseur, M.: Photooxidation of dimethylsulfide (DMS) in the Canadian Arctic, Biogeosciences, 10, 6793–6806, https://doi.org/10.5194/bg-10-6793-2013, 2013.

Tashmim, L., Porter, W. C., Bertram, T. H., Kilgour, D. B., and Rollins, A.: Global Impacts of Marine Methanethiol Emissions and Chemistry in the Atmosphere, Environmental Science & Technology, 59, 20 421–20 428, https://doi.org/10.1021/acs.est.5c02019, publisher: American Chemical Society, 2025.

Teng, Z.-J., Qin, Q.-L., Zhang, W., Li, J., Fu, H.-H., Wang, P., Lan, M., Luo, G., He, J., McMinn, A., Wang, M., Chen, X.-L., Zhang, Y.-Z., Chen, Y., and Li, C.-Y.: Biogeographic traits of dimethyl sulfide and dimethylsulfoniopropionate cycling in polar oceans, Microbiome, 9, 207, https://doi.org/10.1186/s40168-021-01153-3, 2021.

Thomalla, S. J., Nicholson, S.-A., Ryan-Keogh, T. J., and Smith, M. E.: Widespread changes in Southern Ocean phytoplankton blooms linked to climate drivers, Nature Climate Change, 13, 975–984, https://doi.org/10.1038/s41558-023-01768-4, publisher: Nature Publishing Group, 2023.

Tison, J.-L., Brabant, F., Dumont, I., and Stefels, J.: High-resolution dimethyl sulfide and dimethylsulfoniopropionate time series profiles in decaying summer first-year sea ice at Ice Station Polarstern, western Weddell Sea, Antarctica, Journal of Geophysical Research: Biogeosciences, 115, https://doi.org/10.1029/2010JG001427, _eprint: https://agupubs.onlinelibrary.wiley.com/doi/pdf/10.1029/2010JG001427, 2010.

Trevena, A. J. and Jones, G. B.: Dimethylsulphide and dimethylsulphoniopropionate in Antarctic sea ice and their release during sea ice melting, Marine Chemistry, 98, 210–222, https://doi.org/10.1016/j.marchem.2005.09.005, 2006.

van den Berg, A., Turner, S., van Duyl, D., and Ruardij, P.: Model structure and analysis of dimethylsulphide (DMS) production in the southern North Sea, considering phytoplankton dimethylsulphoniopropionate- (DMSP) lyase and eutrophication effects, Marine Ecology Progress Series, 145, 233–244, https://doi.org/10.3354/meps145233, 1996.

Vance, T. R., Davidson, A. T., Thomson, P. G., Levasseur, M., Lizotte, M., Curran, M. A. J., and Jones, G. B.: Rapid DMSP production by an Antarctic phytoplankton community exposed to natural surface irradiances in late spring, Aquatic Microbial Ecology, 71, 117–129, https://doi.org/10.3354/ame01670, 2013.

von Glasow, R. and Crutzen, P. J.: Model study of multiphase DMS oxidation with a focus on halogens, Atmospheric Chemistry and Physics, 4, 589–608, https://doi.org/10.5194/acp-4-589-2004, publisher: European Geosciences Union, 2004.

https://doi.org/10.5194/egusphere-2026-1346
Preprint. Discussion started: 13 April 2026

Wang, S., Yan, J., Lin, Q., Zhang, M., Xu, S., Zhao, S., and Ruan, M.: Formation of marine secondary aerosols in the Southern Ocean, Antarctica, Environmental Chemistry, 18, 285–293, https://doi.org/10.1071/EN21068, publisher: CSIRO PUBLISHING, 2021.

Watts, S. F. and Brimblecombe, P.: The Henry's law constant of dimethyl sulphoxide, Environmental Technology Letters, 8, 483–486, https://doi.org/10.1080/09593338709384509, publisher: Taylor & Francis _eprint: https://doi.org/10.1080/09593338709384509, 1987.

Webb, A. L., van Leeuwe, M. A., den Os, D., Meredith, M. P., J. Venables, H., and Stefels, J.: Extreme spikes in DMS flux double estimates of biogenic sulfur export from the Antarctic coastal zone to the atmosphere, Scientific Reports, 9, 2233, https://doi.org/10.1038/s41598-019-38714-4, publisher: Nature Publishing Group, 2019.

Wohl, C., Villamayor, J., Galí, M., Mahajan, A. S., Fernández, R. P., Cuevas, C. A., Bossolasco, A., Li, Q., Kettle, A. J., Williams, T., Sarda-Esteve, R., Gros, V., Simó, R., and Saiz-Lopez, A.: Marine emissions of methanethiol increase aerosol cooling in the Southern Ocean, Science Advances, 10, eadq2465, https://doi.org/10.1126/sciadv.adq2465, publisher: American Association for the Advancement of Science, 2024.

Wohl, C., Forster, G. L., Edwards, P. M., Suntharalingam, P., and Oram, D. E.: Methanethiol Abundance and Oxidation in a Polluted Marine Atmosphere, Geophysical Research Letters, 52, e2025GL114 929, https://doi.org/10.1029/2025GL114929, _eprint: https://onlinelibrary.wiley.com/doi/pdf/10.1029/2025GL114929, 2025.

Wright, S. W., van den Enden, R. L., Pearce, I., Davidson, A. T., Scott, F. J., and Westwood, K. J.: Phytoplankton community structure and stocks in the Southern Ocean (30–80°E) determined by CHEMTAX analysis of HPLC pigment signatures, Deep Sea Research Part II: Topical Studies in Oceanography, 57, 758–778, https://doi.org/10.1016/j.dsr2.2009.06.015, 2010.

Zang, C. L. and Willis, M. D.: Deployment and evaluation of an NH4+ H3O+ reagent ion switching chemical ionization mass spectrometer for the detection of reduced and oxygenated gas-phase organic compounds, Atmospheric Measurement Techniques, 18, 17–35, https://doi.org/https://doi.org/10.5194/amt-18-17-2025, 2025.

Zhang, M., Park, K.-T., Yan, J., Park, K., Wu, Y., Jang, E., Gao, W., Tan, G., Wang, J., and Chen, L.: Atmospheric dimethyl sulfide and its significant influence on the sea-to-air flux calculation over the Southern Ocean, Progress in Oceanography, 186, 102 392, https://doi.org/10.1016/j.pocean.2020.102392, 2020.

Zhang, Y., Sun, J., Shen, X., Lal Chandani, V., Du, M., Song, C., Dai, Y., Hu, G., Yang, M., Tilstone, G. H., Jordan, T., Dall'Olmo, G., Liu, Q., Nemitz, E., Callaghan, A., Brean, J., Sommariva, R., Beddows, D., Langford, B., Bloss, W., Acton, W., Harrison, R., Dall'Osto, M., and Shi, Z.: Measurements of particulate methanesulfonic acid above the remote Arctic Ocean using a high resolution aerosol mass spectrometer, Atmospheric Environment, 331, 120 538, https://doi.org/10.1016/j.atmosenv.2024.120538, 2024.

Zhou, S., Chen, Y., Huang, S., Gong, X., Yang, G., Zhang, H., Herrmann, H., Wiedensohler, A., Poulain, L., Zhang, Y., Wang, F., Xu, Z., and Yan, K.: A 20-year (1998–2017) global sea surface dimethyl sulfide gridded dataset with daily resolution, Earth System Science Data, 16, 4267–4290, https://doi.org/https://doi.org/10.5194/essd-16-4267-2024, 2024.